Theoretical Insights on Chain Growth Mechanisms in Fischer-Tropsch Synthesis at High CO Coverage on Ru Particles

A Thesis

Presented to

the faculty of the School of Engineering and Applied Science

University of Virginia

in partial fulfillment

of the requirements for the degree

Master of Science

by

Thomas Lawlor

Approval Sheet

The thesis

is submitted in partial fulfillment of the requirements

for the degree of

Master of Science

_____

Author

The thesis has been read and approved by the examining committee

_____

Advisor

_____

_____

_____

Accepted for the School of Engineering and Applied Science

Dean, School of Engineering and Applied Science

April

2017

Abstract

The global demand for energy is projected to increase by over 70% by 2050 [43] . Such demands coupled with decreasing oil reserves will ultimately require sustainable strategies for the production of clean fuels. Fischer Tropsch Synthesis (FTS) is a well-established industrial process that can be used to convert syngas derived from emerging energy sources such as natural gas and biomass feedstocks into fuels and chemicals [1,2,3,4]. FTS involves the activation of CO in the presence of hydrogen to form hydrocarbon monomers that subsequently polymerize to form n-alkanes, 1-alkenes, aldehydes and alcohols. The reaction is typically carried out on group VIII metals including Fe, Co, Ru, Rh and Ni [1,2,3,5]. Despite decades of research the mechanisms involved in C-O activation and C-C bond formation are still actively debated. First-principle density functional theory (DFT) calculations were carried out herein to investigate the elementary C-C bond formation and chain propagation pathways over the model (111) terrace sites of a 119 atom Ru cluster chosen to mimic the active sites of large supported Ru clusters. The calculations were carried out at full monolayer coverages of CO to appropriately capture the high coverage conditions that are used industrially as well as in the laboratory. Both the CO insertion and carbene or "CH_x insertion" mechanisms were explored. Plausible chain propagation paths via the CO insertion mechanism were explored including comparisons of direct versus hydrogen-assisted activation of CH_xC-O*. The addition of hydrogen to oxygen lowered the free energy of the transition states for C-O scission in comparison with routes involving direct C-O bond activation in all cases irrespective of the saturation of the CH_x* species. Simulation results indicate that the chain propagation for CO insertion proceeds via the addition of surface hydrogen (H*) to the

oxygen atom of adsorbed CH_3CO^* in an irreversible step that controls the selectivity with an overall activation barrier ~ 140 kJ mol^{-1} relative to adsorbed methylidyne (CH*). Chain propagation for the CH_x insertion mechanism preferentially proceeds via carbon-carbon coupling of two alkylidyne surface intermediates or by the combination of an alkylidyne with an alkylidene intermediate with low free energy barriers ~70 kJ mol^{-1} relative to two adsorbed CH*. While the resulting energetics reported herein indicate that CH_x insertion is energetically much more favorable than CO insertion, the kinetics associated with the probability of CH_x intermediates finding one another in the dense CO adlayer may limit such paths.

Table of Contents

Chapter 1 –Introduction

The increasing global demand for energy has increased the importance of developing new strategies to produce fuels to meet these demands in a more sustainable manner that does not rely on petroleum resources alone. Fischer Tropsch Synthesis (FTS) is a well-established industrial process that can be used to convert syngas (a mixture of CO and H_2) derived from emerging energy sources such as natural gas and biomass feedstocks into fuels and chemicals [1,2,3,4].

FTS involves the activation of CO in the presence of hydrogen to form hydrocarbon monomers that subsequently polymerize to form n-alkanes, 1-alkenes, aldehydes and alcohols. The reaction is typically carried out on group VIII metals including Fe, Co, Ru, Rh and Ni [1,2,3,5]. Ni based FT catalysts tend to produce mainly methane [3, 5]. Ru is considered the most active metal for FTS making it ideal for fundamental studies in a laboratory setting but its high market price makes it economically inefficient for commercial use. Cobalt and iron based catalysts are the catalysts of choice in practice as they are active and very cheap [3]. The overall stoichiometric reactions to form paraffins and olefins from syngas are given below in equations 1 and 2.

$$nCO + (2n+1)H_2 \rightarrow C_nH_{2n+2} + nH_2O \quad (1)$$

$$nCO + 2nH_2 \rightarrow C_nH_{2n} + nH_2O \quad (2)$$

Despite decades of research studies, the fundamental mechanisms that control FTS are still actively debated [5,6,7,8,9,10].

FTS, being a polymerization reaction, is characterized by initiation, chain growth, and chain termination reactions. The product distribution that forms from reaction tends to follow the Anderson-Schulz-Flory (ASF) distribution given below in equation (3)

$$F_n = n(1-\alpha)^2 \alpha^{n-1} \quad (3)$$

Here F_n is the fraction of the carbon atoms in chains of length n and α represents the constant probability of adding a monomer to the growing chain, a parameter which is independent of the size of the chain to which the monomer adds. In practice, there are often significant deviations between the idealized ASF distribution and the FTS product distribution. Most catalysts tend to report a negative deviation of α for the lower molecular weight products, and a positive deviation for the heavy products [3,11, 12]. It has been proposed that lighter α-olefins like ethylene tend to readsorb to the catalyst surface and participate in secondary chain growth reactions. An increase in the residence time increases the likelihood of readsorption of α-olefins which tend to increase the observed selectivity of the reaction to form C_{5+} due to an increase in secondary chain growth reactions occuring [11, 12, 13, 14].

An alternative approach towards modeling the FT product distribution was used by Iglesia et al. and was originally developed by Herrington to describe the product distribution in terms of the individual chain termination parameter β_n given below in equation 4, whose value depends on the size of the growing chain [11, 12, 13,16].

$$\beta_n = \frac{r_{t,n}}{r_{p,n}} = \frac{\phi_n}{\sum_{i=n+1}^{\infty} \phi_i} \quad (4)$$

Here the rate $r_{t,n}$ represents the total chain termination rate for carbon chains of length n. The rate $r_{p,n}$ represents the rate of propagation, i.e. the rate at which the monomer adds to the growing chain to form a surface bound chain of length n+1. The symbol φ_n represents the mole fraction of chains of length n on the surface. The individual chain growth probability α_n and its relation to β_n is given below in equation 5.

$$\alpha_n = \frac{r_{p,n}}{r_{p,n} + r_{t,n}} = \frac{\sum_{i=n+1}^{\infty} \phi_i}{\sum_{i=n}^{\infty} \phi_i} = \frac{1}{1+\beta_n} \qquad (5)$$

The terms in equation 5 have the same meaning as described above.

The first step in FTS, initiation, begins via the activation of the C-O bond of a chemisorbed CO surface intermediate (CO*). Recent kinetic and theoretical studies have shown that CO* is likely activated through hydrogen assisted pathways during FTS on Ru and Co catalysts [6,8,9,10] where hydrogen is first added to CO*. The addition of hydrogen to CO transfers electrons into the antibonding $2\pi^*$ states on CO*. This activates the C-O bond and lowers its barrier to dissociate and form adsorbed methylidyne (CH*) and hydroxyl (OH*) intermediates. The experimentally measured CO consumption rate reported by Iglesia et al. show that the rates increase linearly with increasing hydrogen pressure and decrease linearly with CO [6,8,9]. The results suggest that CO covers the surface where $KP_{CO} >> 1$ and the rate can be well-modeled by equation (6) [6,8,9,10].

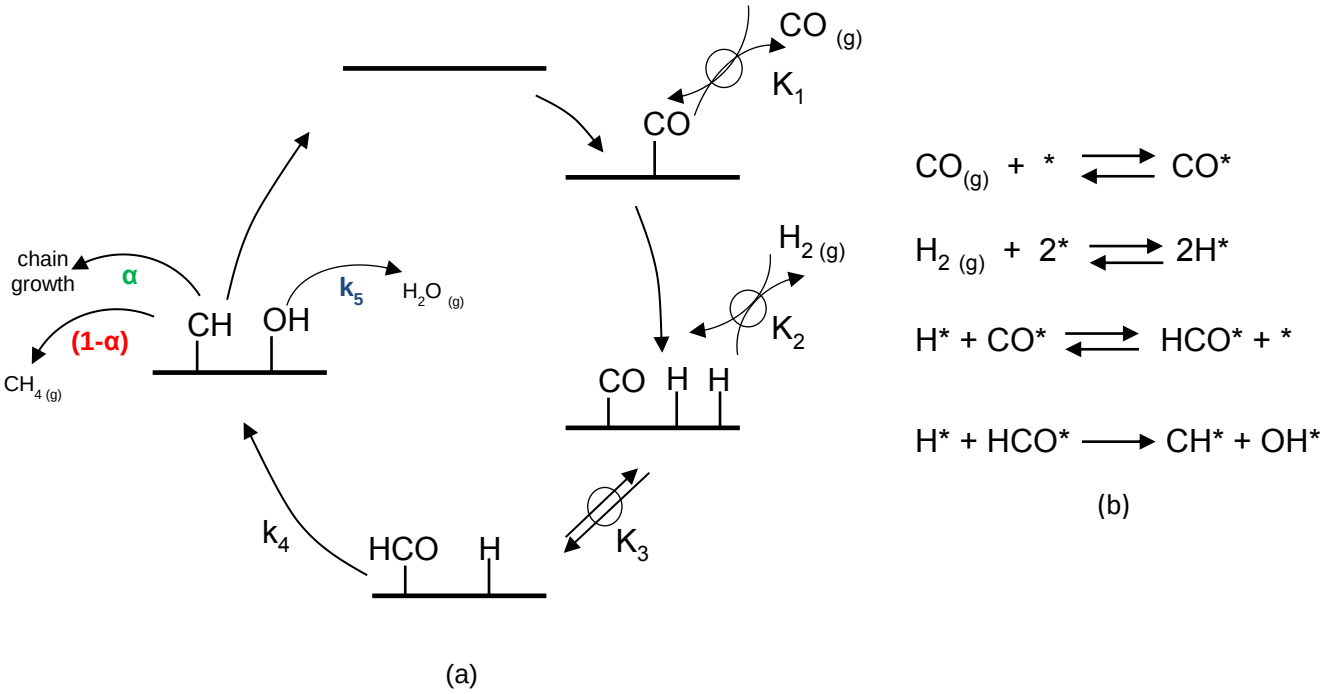

Figure 1 Elementary steps associated with H*-assisted C-O activation expressed as (a) catalytic cycle (b) chemical equations.

$$r_{CO} = \frac{K_1 K_2 K_3 k_4 P_{co} P_{H_2}}{(1 + K_1 P_{co})^2} \qquad (6)$$

The elementary steps used to derive equation 6 are shown in Figure (1-a). Here K_1 and K_2 are the equilibrium constants for CO and H_2 adsorption, respectively. K_3 is the equilibrium constant for the first addition of H* to CO* to form HCO* and is considered a quasi-equilibrated step and is shown in Figure (1-a). The rate constant k_4 is the constant for the reaction involving H* addition to the formyl group (HCO*) which is assumed to be the irreversible and rate determining step in this scheme for the H*-assisted activation of CO*. The experimental CO consumption rates reported on Ru and Co [6,8,9,17] depend linearly on the partial pressure of hydrogen p_{H_2} and show a negative order dependence on CO at higher CO partial pressures where $K_{co}P_{CO} >> 1$. The results support the hydrogen-assisted C-O activation mechanism and the observed linear dependence of the CO consumption rate on the hydrogen pressure reflects the fact that two hydrogen addition steps are required to activate C-O [6,8,9,10].

Mechanisms involving direct C-O activation without the assistance of adsorbed hydrogen do not appear to be consistent with measured CO consumption rates that depend linearly on hydrogen pressure [6,8,9,17]. van Santen et al. have carried out calculations at low CO coverages for C-O activation at the B5 step edge sites and reported an activation barrier ~ 60 kJ mol^{-1} on Ru [5] which would indicate that CO can dissociate at these sites. These sites, however, are very active and under FTS conditions they are likely covered with either CO or dissociate fragments. More recent DFT calculations for the direct C-O activation at B5 sites of Ru particles at high CO* coverage have shown that the barriers to activate CO directly are nearly 300 kJ mol^{-1} and thus unlikely reactions to occur [8]. Theory has shown that the coordinatively unsaturated metal sites such as step-edge sites and corner sites on metal particles can adsorb more than one CO* molecule. Infrared studies show the formation of both gem di- and tri-carbonyls and supramonolayer CO* coverages even at CO partial pressures much lower than required for FTS [8].

The initial C-O activation results in the formation of the monomers required for chain growth. These chains are thought to grow rapidly and ultimately form alkene and alkane products via chain termination steps. Various C-C bond forming mechanisms have been proposed. The two most highly cited are the CO and "CH_x insertion" mechanisms [1,2.3,5,9,18,19, 27]. Figure (2-a) shows a version of a CH_x insertion mechanism which was originally proposed by Brady and Petit[5,18,19], where chain growth occurs via the polymerization of methylene (-CH_2-) groups on the surface. Figure (2-b) is a more elaborate CH_x insertion mechanism known as the alkenyl mechanism, originally proposed by Maitlis [20,21,22]. In this mechanism CH* combines with CH_2* to form a vinyl group (HC-CH_2*) on the surface which subsequently undergoes C-C bond

formation by adding an additional methylene group. The C-C bond formation step is followed by a hydrogen shift isomerization step to form a growing vinyl chain on the surface. This process continues until termination to alkenes and alkanes occurs via subsequent hydrogen addition steps. This mechanism was supported by studies of C-C coupling in homogeneous systems, as well as the co-feeding of vinyl probes and the observation that these vinyl probes were able to adsorb to the surface and become incorporated into longer chain FT products [21,22,23]. Figure (2-c) shows a schematic of the CO insertion mechanism initially proposed by Pichler and Schulz [5]. The mechanism involves alkyl CO insertion followed by the activation of C-O bond with H_2. The CO insertion mechanism has been proposed to explain the fact that FTS typically produces a small amount of oxygenates, it also appears to be consistent with rapid chain growth because CO* being the most abundant surface intermediate (MASI) under reaction conditions, would ensure that the monomer is readily available once the chain growth event is initiated.

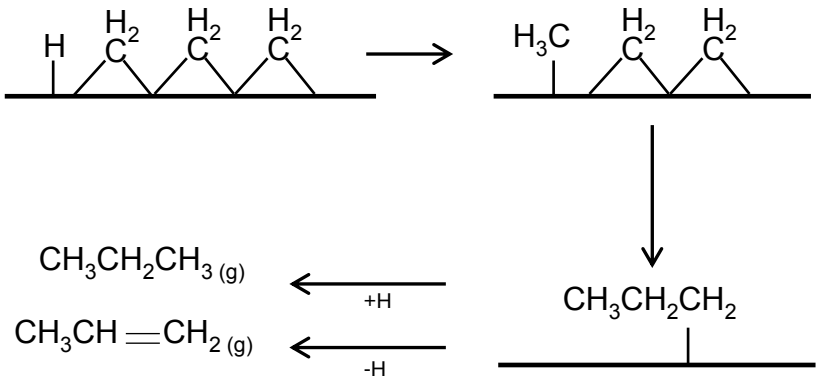

(a)

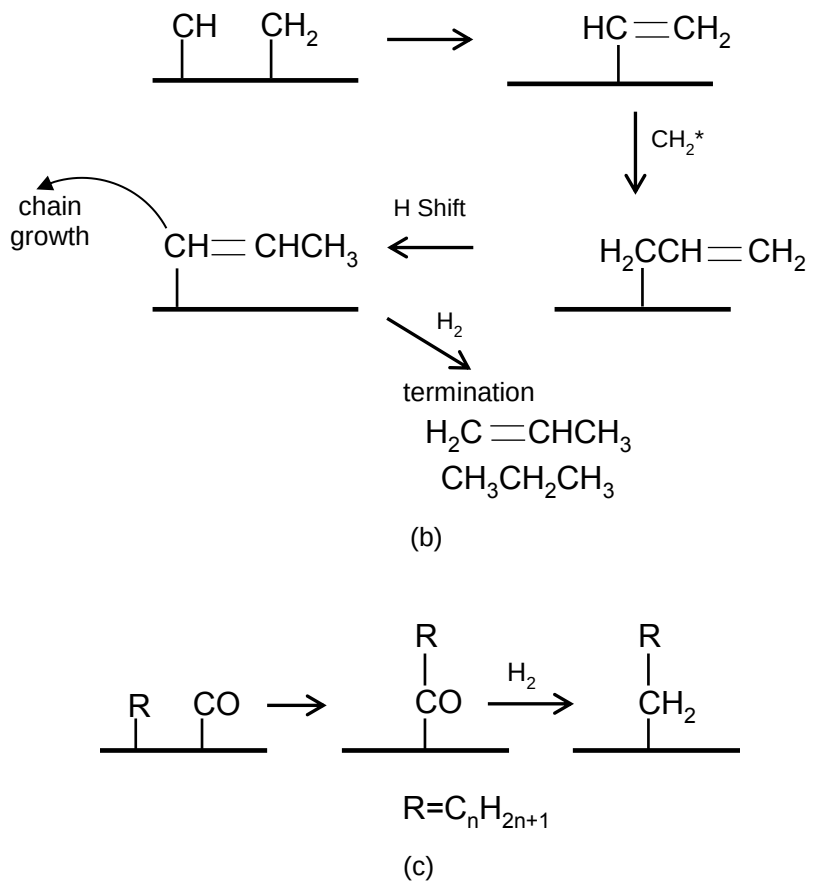

Figure 2: Commonly proposed chain-growth mechanisms in FTS (a) Methylene polymerization (b) Alkenyl chain growth mechanism proposed by Maitlis (c) Alkyl CO Insertion.

Despite the amount of research that has been done related to FT, both experimental and theoretical, many fundamental questions about the reaction mechanism are unanswered; at present the identity of the monomer is unknown and the precise nature of the chain growth mechanism is still a topic of active research and considerable debate. Ultimately, theory and experiments will need to be used synergistically to unravel the FTS mechanism.

While DFT has been used to examine the plausible CO activation and C-C bond formation paths relevant to FTS as reported in the literature [5,6,7,23,24,25,26,27] these studies have invariably

used flat planar single crystal surfaces with CO* coverages well below a stoichiometric monolayer [5,6,23,24,25,26,27].

More recent studies have used curved Ru_{201} cubooctahedral particles to study C-O activation at CO* coverages of 1 ML [8,9,10]. That these models may be a better representation of the metal nanoparticles which catalyze FTS is suggested by kinetic studies which indicate that the CO consumption rate is of negative order in CO, indicating that CO is the most abundant surface intermediate (MASI) under reaction conditions.[6,8,9,10,14,17]. Additionally, recent studies have shown IR bands consistent with a surface coverage of CO* >1 ML even at CO partial pressures lower than that used for FTS in practice [8]. DFT studies at high CO* coverage on such particles have shown that of the different coordinated Ru atoms present on the cubooctahedral particle (CN 6-9) that the Ru atoms with higher coordination number which represent the Ru atoms on the low-index face of the (111) terrace are able to activate CO most easily. The reason the Ru atoms on the (111) terrace sites are most active for C-O activation during FTS is because the CO* is bound least strongly at those sites and is more likely to desorb from those sites forming "a vacancy" next to a vicinal CO* which can subsequently be activated by H_2 [6,8,9,10].

The (111) terraces represent a greater fraction of the exposed surface Ru atoms on larger cubooctahedral particles. According to the model it follows that CO activation, and hence the CO consumption rate would be expected to increase with increasing particle diameter as a greater fraction of the surface is now made up of active sites, This is consistent with what has been reported in the literature demonstrating particle size effects observed for the reaction in the range of particles < 10 nm [29,30].

The work herein explored C-C bond formation paths via CO insertion and CH_x insertion mechanisms on the (111) terrace sites of a Ru_{119} half particle model. High CO* coverage influences the binding energy and hence the reactivity of bound surface intermediates in concentrations likely to be present on the catalyst surface during reaction conditions and should be used in theoretical models to investigate FTS under the high partial pressures of CO required for long chain selectivity and where (CO*) ~ 1.

Chapter 2 –Computational Methods

All calculations reported in the study herein were carried out using plane wave gradient corrected density functional theory (DFT) using the Vienna Ab Initio Software Package (VASP) developed by Kresse and Hafner [31]. The Kohn Sham equations were solved using a plane wave basis set with a kinetic energy cutoff of 396 eV to determine the electronic structure of the system [32]. The generalized gradient approximation (GGA) was used along with the revised Perdew-Burke-Ernzerhof (RPBE) functional to determine exchange-correlation and the corresponding energies [33]. The ionic cores were described using Vanderbilt ultrasoft pseudopotentials (USPP) [34].

The upper half of a Ru_{201} particle (Ru_{119} half cluster) was used to model the hydrogenation and C-C bond formation. Fischer-Tropsch synthesis is typically carried out at over 10 atmospheres of CO pressure where the surfaces are thought to be fully covered in CO. Herein we examine the plausible FTS chain growth reaction pathways on a 1 ML CO covered Ru_{119} cluster. In this model, a CO* coverage of 1 ML refers to one CO molecule occupying each available surface Ru atom as shown below in Figure 3. The half particle with 1 ML of CO* was generated by first optimizing a full Ru_{201} particle with 1 ML CO* coverage to full convergence. The bottom 3 rows of Ru atoms (82 Ru atoms) and the associated CO* molecules were subsequently removed from the full particle to generate the Ru_{119} "half cluster" which was computationally much more feasible to investigate the plausible reaction pathways and perform transition state searches. The 119 Ru cluster has 70 atoms that are exposed at the surface. The bottom two layers of Ru in this structure and their associated CO* were held fixed in their optimized positions, in order to avoid interactions with the vacuum space in the unit cell below the particle and as a way to maintain the symmetry of the full cubooctahedral particle. The top 2 layers of Ru atoms in the half

particle, the chemisorbed CO* as well as all other reactive intermediates were allowed to relax during energy optimizations and transition state searches. The half particle model resulted in changes in the differential binding energy of $CO_{(g)}$ of < 2 kJ mol^{-1} when compared to the full Ru_{201} particle at 1 ML CO* coverage which is less than the error of the method and provided verification that it was a faithful representation of the full particle model. A single Γ-centered k point was used to integrate over the first Brillouin zone with a unit cell size of 28 x 28 x 18 $Å^3$[35]. Calculations carried out with a larger 30 x 30 x 20 $Å^3$ unit cell resulted in a difference of differential CO binding energies of < 2 (kJ/mol) which is less than the intrinsic error in the method. The wave functions and charge density were optimized until they varied by < 10^{-4} eV and the geometric structure was optimized until the forces on all atoms was < 0.05 eV $Å^{-1}$. Calculations carried out at the higher convergence criteria of < 0.01 eV $Å^{-1}$ resulted in CO binding energies as well as reaction energies of < 3 kJ mol^{-1} and thus reliable for the subsequent calculations.

.

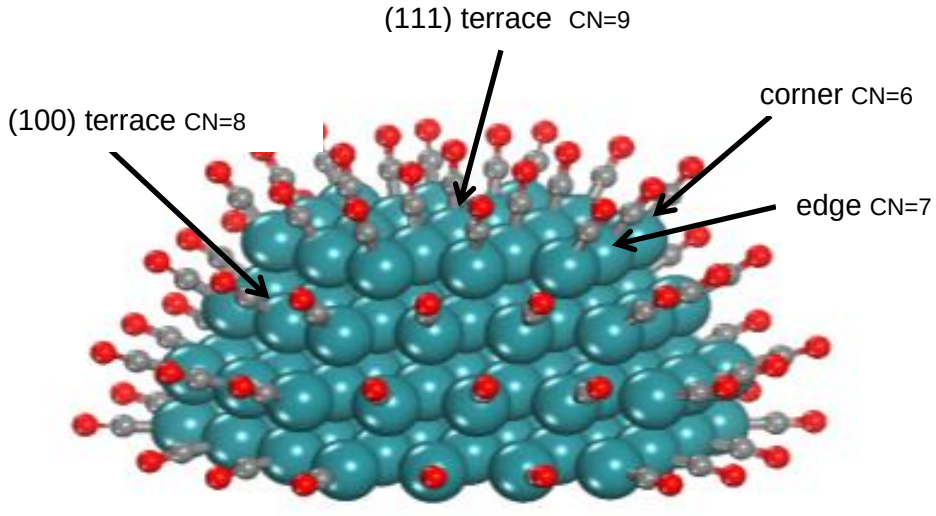

Figure 3: (a) The model Ru_{119} half cluster with 1 monolayer CO coverage showing different facets and Ru coordination number.*

The nudged elastic band (NEB) method was used to find reaction pathways by linear interpolation between the converged reactant and product structures with a set of (8 or 16 images)[36,37,38,39]. The highest energy point along the optimized reaction path was used as an input for a more detailed transition state search using the dimer method. The dimer method takes two images from the minimum energy path (MEP) determined from the NEB method and uses them to construct a "dimer" which is displaced along the potential energy surface until a saddle point is found and the forces on all atoms were less than 0.05 eV $Å^{-1}$ [38,40].

The binding energies of adsorbates were calculated using the following equation

$$\Delta E = E_{Ru+Ads} - (E_{Ru} + E_{Ads(g)}) \quad (7)$$

where E_{Ru+Ads} refers to the energy of the particle with the adsorbate, E_{Ru} is the energy of the particle without the adsorbate and $E_{Ads\ (g)}$ is the energy of the adsorbate in the gas phase.

The activation barriers for elementary steps were calculated using equation (8).

$$E_{act} = E_{TS} - E_{\mathrm{R}} \quad (8)$$

where E_{act} is the activation barrier E_{TS} is the energy of the transition state and E_R is the energy of the reactant state. The energy of reaction is the difference in energy between the reactant and product states and is calculated by equation (9).

$$\Delta E_{Rxn} = E_P - E_{\mathrm{R}} \quad (9)$$

The energies reported in equations 7-9 provide reliable intrinsic information about the reaction. In order to analyze the full sequence of elementary steps for propagation and termination and to determine the most favorable chain propagation reaction pathway(s) we calculated the free

energies for each of the elementary steps. In order to compare the energies of different states, we use the energy of the fully CO covered Ru particle along with a single molecule of $H_{2\,(g)}$ in the gas phase and one CH* intermediate bound to a threefold hcp site on the (111) terrace as a reference state to compare chain growth mechanisms. This model appears to be consistent with the kinetic and infrared FT experiments discussed earlier [6, 8, 9]. It provides a model "snapshot" of what the catalyst surface may look like just after chain initiation, which occurs via, hydrogen-assisted C-O bond activation, and just prior to C-C bond formation. Therefore, elementary steps involving hydrogen-addition also include the free energy of adsorption, ΔG_{ads} for $H_{2\,(g)}$ where ΔG_{ads} is given by:

$$\Delta G_{ads} = \Delta H_{ads} - T\Delta S_{ads} \qquad (10)$$

ΔS_{ads} refers to the standard gas phase entropy of hydrogen as published by NIST [41]. The enthalpy of adsorption, $\Delta H_{ads,}$ for hydrogen was estimated by using the binding energy of H* on the particle model as calculated by DFT and referenced to the DFT calculated energy for $H_{2\,(g)}$. The free energy of activation and the free energy of reaction for the elementary H* addition steps were obtained by adding ΔG_{ads} to the intrinsic DFT calculated activation and reaction energies.

Chapter 3 –Results and Discussion

Adsorption Energies of Reactive Intermediates

The binding energies for CO and all of the hydrogenated C_1 fragments were calculated at different sites on the (111) terrace of the Ru particle at 1 ML CO* coverage the results are given in Table 1. CH_3* appears to bind the weakest to the Ru surface with a binding energy of 68 kJ mol^{-1}. The weak binding energy of CH_3* is the result of a combination of repulsive interactions between the bulky methyl group and the dense CO* adlayer surrounding it; and the fact that CH_3* prefers to bind in the "atop" configuration which means that it forms only a single Ru-C (with a bond length of 2.18 Å). Carbon monoxide also prefers to bind in the atop configuration, with an Ru-C bond length of 1.92 Å which is shorter than the Ru-C bond of CH_3*. This reflects a stronger Ru- CO over the Ru-CH_3 bond. This is consistent with the calculated binding energies of 118 kJ mol^{-1} for CO* vs 68 kJ mol^{-1} for CH_3* . The CH_2* methylidene intermediate prefers to sit in bridge sites on the surface and forms 2 Ru-C bonds (averaging 2.06 Å) and has a binding energy of 330 kJ mol^{-1}. The more unsaturated methylidyne (CH*) intermediate is the most strongly bound CHx* intermediate on the Ru surface. It preferentially binds to the threefold hollow site and has a binding energy of 546 kJ mol^{-1} forming three Ru-C bonds (averaging 2.02 Å).

The relative binding energies of intermediates provides some insight into relative migration energies for these intermediates and their ability to diffuse and react with adsorbed CO* and other CH_x* intermediates via CO* and CH_x* insertion steps. For CO* insertion with CH* and CH_2*, the more weakly held CO* migrates toward strongly bound and less mobile CH* and CH_2* intermediates prior to the insertion of CO* into the metal-CH_x bond. In the reaction between CO* and CH_3*, the more weakly held CH_3* alkyl intermediate migrates to the bound

CO* and inserts into the Ru-CO bond rupturing the Ru-CH_3 bond upon the formation of the C-C bond with a CO*. In the case of C-C bond formation via CH_x insertion routes, the more saturated CH_x* intermediate prefers to migrate towards the more strongly bound, less saturated, CH_y* on the surface.

Table 1: Binding energies of reactive intermediates CO, CH_x* (x= 1-3) on (111) terrace sites of Ru_{119} half particle at 1ML CO* coverage values reported in kJ mol^{-1}*

Adsorbate	Binding Energy kJ mol^{-1}	Configuration
CO*	118	atop
CH*	546	threefold
CH_2*	330	bridge
CH_3*	68	atop

CO Insertion and Hydrogenation of Methylidyne

The relative concentration of the reactive R- CH_x* species that form on the CO-covered Co and Ru surfaces under reaction conditions is thought to be rather low. Isotopic $^{12}CO/^{13}CO$ switching data, however indicate that these species grow rapidly before terminating to form alkene or alkane products [42]. As such, chain growth and termination are controlled by the competition between the C-C bond formation and the hydrogenation of R- CH_x* intermediates which is set by the intrinsic rate constants for these steps and the local surface coverage under reaction conditions. For example, once methylidyne (CH*) is formed, it may react with a vicinal monomer unit to form C_2H_x* or hydrogen to form adsorbed methylene (CH_2*). If chain growth in FTS preferentially proceeds via CO insertion, the monomer unit is CO*, the most abundant surface intermediate (MASI) under reaction conditions as shown by kinetic, IR and theoretical studies of the FT reaction [6,8,9,10].

The calculated reaction energies for the addition of CO* as well as H* to the adsorbed methylidyne (CH*) on the low-index (111) terrace sites of the Ru particle are shown in Figure 4. The activation barrier for CO* insertion (Fig. 4-a) is relatively modest at 65 kJ mol^{-1}. The reaction proceeds via the migration of the more weakly held CO* species towards the more strongly bound CH* intermediate. The C-C bond length in the transition state is calculated to be 1.65 Å. Additional stability is gained in the product state as the terminal oxygen of the CH--CO* intermediate points "inward" to an unoccupied Ru site on the terrace where there it feels fewer repulsive interactions with the dense surrounding CO* adlayer. In the product state (CHCO**) has a C-C bond of 1.45 Å and a C-O bond of 1.21 Å. This step is endothermic with an overall reaction energy of 53 kJ mol^{-1}. The hydrogenation of the CH* methylidyne intermediate to form methylidene (CH_2*) has a rather high activation barrier of 53 kJ mol^{-1} as shown in Figure (4-b). The distance between the carbon atom and the hydrogen atom which added to it in the transition state is 1.57 Å and all three Ru-C bonds remain intact in the transition state structure. The product structure contains two C-H bonds of ~ 1.10 Å and forms methylidene (CH_2*). One of the Ru-C bonds breaks as the hydrocarbon fragment moves from a threefold hollow site initially to a bridge site in the product state. This step is predicted to be slightly endothermic with ΔE_{RXN} = 17 kJ mol^{-1}. The endothermicity here appears to be the result of the increased repulsion of the larger CH_2* product over that of the CO* reactant with the dense CO* adlayer present under FTS conditions.

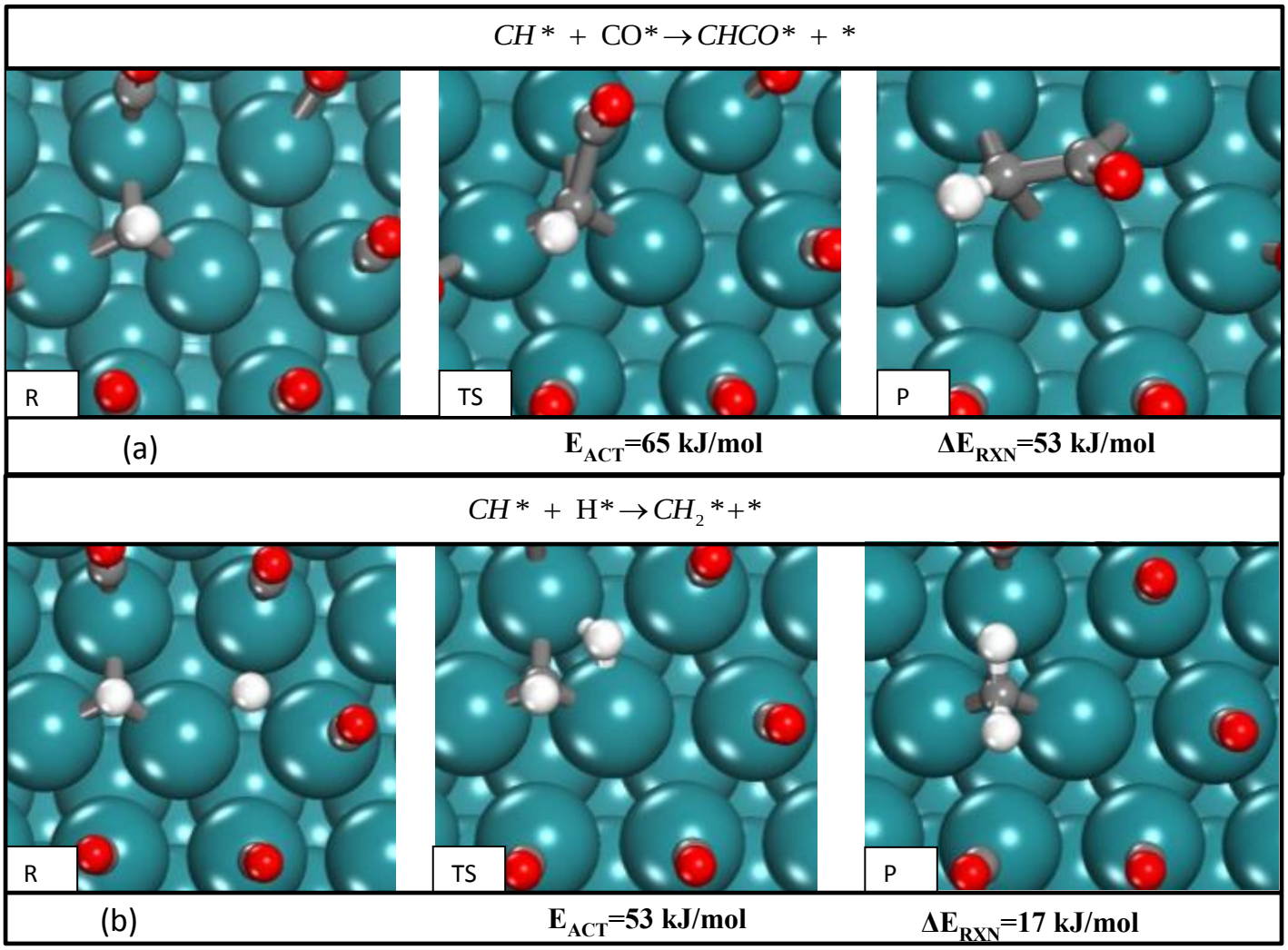

Figure 4: Reaction energies for CO insertion (a) and hydrogenation (b) of methylidyne (CH) on (111) terrace sites of Ru_{119} half particle at 1ML CO* coverage. Ru atoms are teal, oxygen atoms are red, carbon atoms are gray, hydrogen atoms are white.*

CO Insertion and Hydrogenation of Methylidene

The reaction energies for the addition of CO* and H* to form adsorbed methylidene (CH_2*) are reported in Fig. 5. The activation barrier for the CO Insertion reaction, shown in Figure (5-a), is 54 kJ mol^{-1}. The reaction proceeds by the migration of the more weakly held CO* towards the more strongly held CH_2*. The C-C distance decreases from 2.63Å in the reactant state to

1.69 Å in the transition state. In the CH_2CO product state, both carbons become sp2 hybridized where all of the H-C-C and O-C-C bond angles are ~ 120 degrees and lie in the same plane. The C-C bond in the product state is 1.42 Å . The C-O bond elongates to 1.30 Å and the oxygen atom forms a bond with a vacant Ruthenium atom of 2.09 Å . This step is moderately endothermic with a reaction energy (ΔE_{RXN}) of 30 kJ mol^{-1}. The hydrogenation of methylidene to form an adsorbed methyl (CH_3*) species is shown in Figure (5-b). This step proceeds via the migration of H* to chemisorbed CH_2* and results in an early transition state where the H_2C-H distance is 1.64 Å and where the two Ru-C bonds of methylene remain intact. The reaction energy to form the adsorbed methyl product is endothermic with ΔE_{RXN} =34 kJ mol^{-1}. The endothermic nature of this step is in part due to the increased steric repulsion that results in moving from the CH_2* species to a bulkier methyl product that sits atop and lies in the same plane as the CO* adlayer, The initial hydrogen atom sits in a threefold site much closer to the metal surface and as such experiences little repulsion with the adlayer due to its small size.

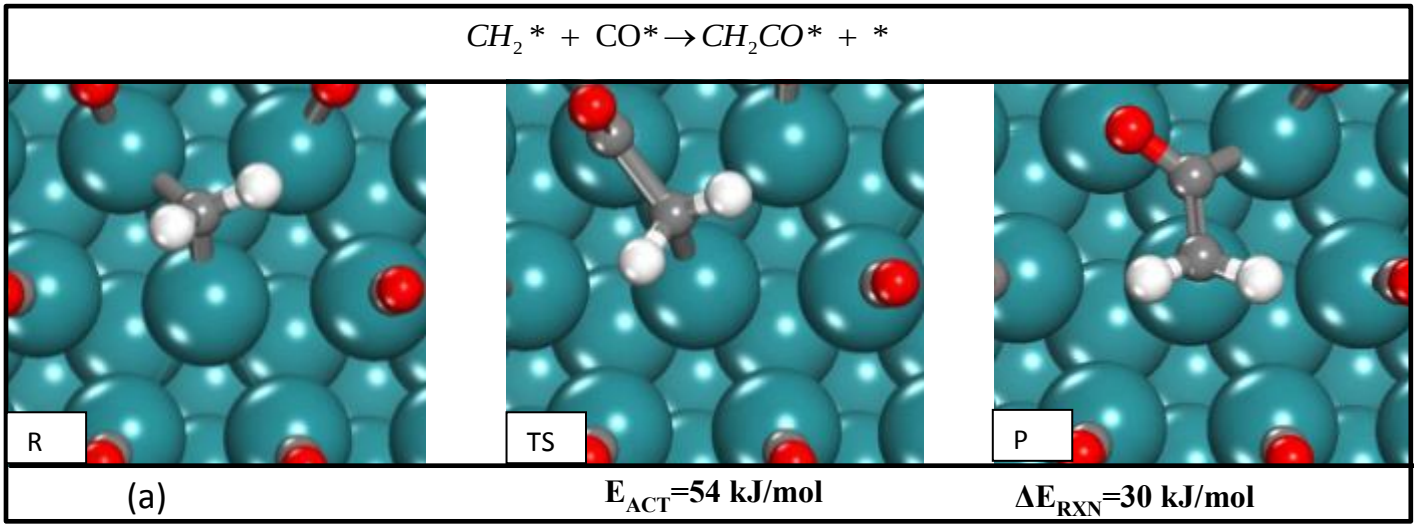

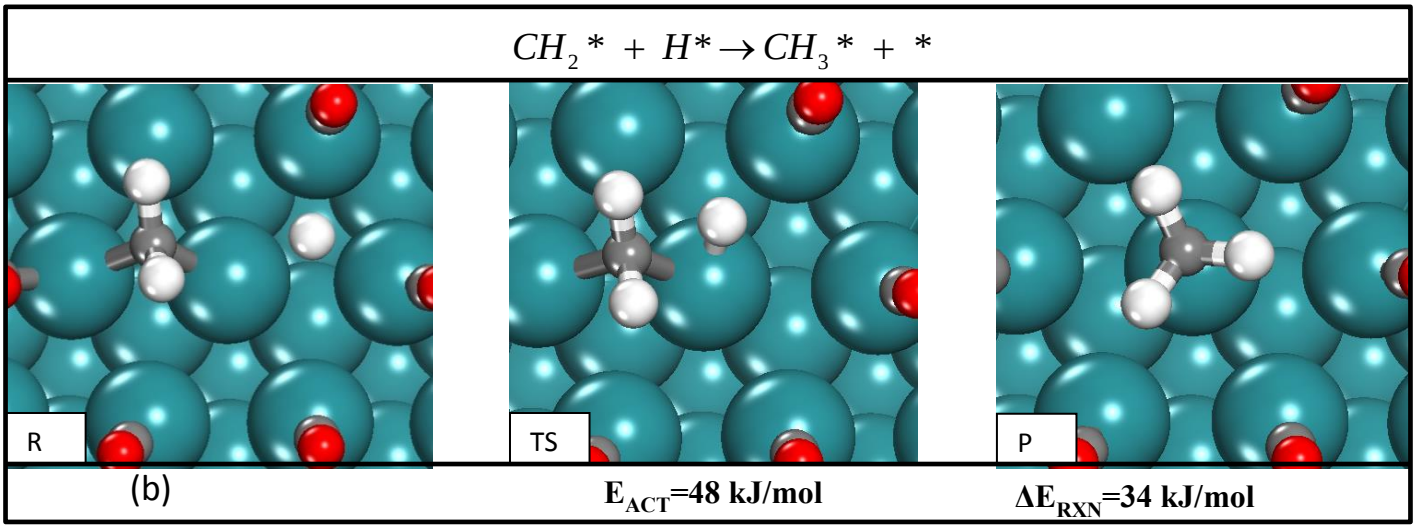

Figure 5: Reaction energies for CO insertion (a) and hydrogenation (b) of (CH_2) on (111) terrace sites of Ru_{119} half particle at 1ML CO* coverage. Ru atoms are teal, oxygen atoms are red, carbon atoms are gray, hydrogen atoms are white.*

CO Insertion and Hydrogenation of Methyl

The methyl (CH_3*) intermediates that form can subsequently react with either CO* or H* to form the surface CH_3CO* intermediate or methane, CH_4 desorbs from the surface upon formation. The CO insertion reaction, shown in Figure (6-a), has a moderate activation barrier of 68 kJ mol^{-1}. The reaction is characteristically different than the reactions of CH*+CO and CH_2*+CO* in that in this system the CH_3* alkyl species actually migrates and inserts into the Ru-CO bond as opposed to CO* migrating and inserting into the Ru-CH_x bond. The preferential migration of the methyl intermediate over that of the CO* is due to the weaker binding energy for Ru-CH_3 verses the Ru-CO. In the transition state for the methyl migration, the Ru-C bond of CH_3* is completely broken and the resulting C-C bond that forms has a bond length of is 1.80 Å. The product of this reaction is an acyl intermediate (CH_3CO*). The alkyl group in the product no longer interacts with the metal surface and points up and away from the surface thus relieving the repulsive interactions with the dense CO adlayer. The resulting C=O bond of the

bound CH_3O^* is significantly weakened via electron donation into antibonding $2\pi^*$ states and a favorable metal-π bond. This results in an elongated C-O bond and strong Ru-C (C (2.03 Å) and Ru-O (2.15 Å) interactions as the CH_3C-O* binds in an η_1 -C η_1-O configuration. This step is calculated to be exothermic with ΔE_{RXN} = -33 kJ mol^{-1}. This is in part due to the favorability of strong metal-π bond interactions and in addition the release of the repulsive interactions between the methyl group and CO adlayer as the CH_3 is pushed above the adlayer in the product state.

The competing reaction which involves the hydrogenation of CH_3* to methane is shown in Figure (6-b). The reaction proceeds via the insertion of H into the Ru-CH_3 bond. The transition state has a C-H bond distance of 1.68 Å and a Ru-C bond of 2.29 Å, and a resulting activation energy of 18 kJ mol^{-1}. The high coverages result in weak Ru-CH_3 and Ru-H interactions which lower the intrinsic barrier for hydrogenation. In addition, the elongation of the Ru-CH_3 bond in the transition state helps to lower the activation energy as this relieves part of the repulsion of the CH_3* and CO* adlayer. The methane that is produced in the product state is desorbed from the surface as the Ru-C distance in the product state is ~ 5.40 Å. This step is highly exothermic, ΔE_{RXN} =-142 kJ mol^{-1} demonstrating that chain termination to n-alkanes is an irreversible step.

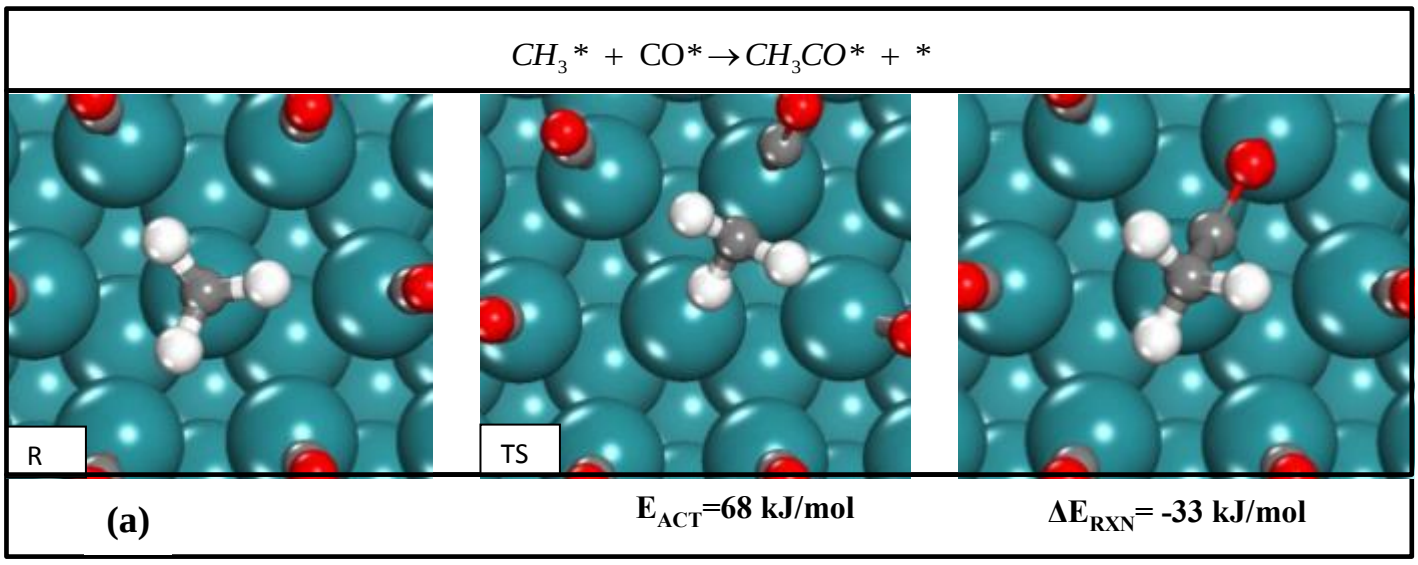

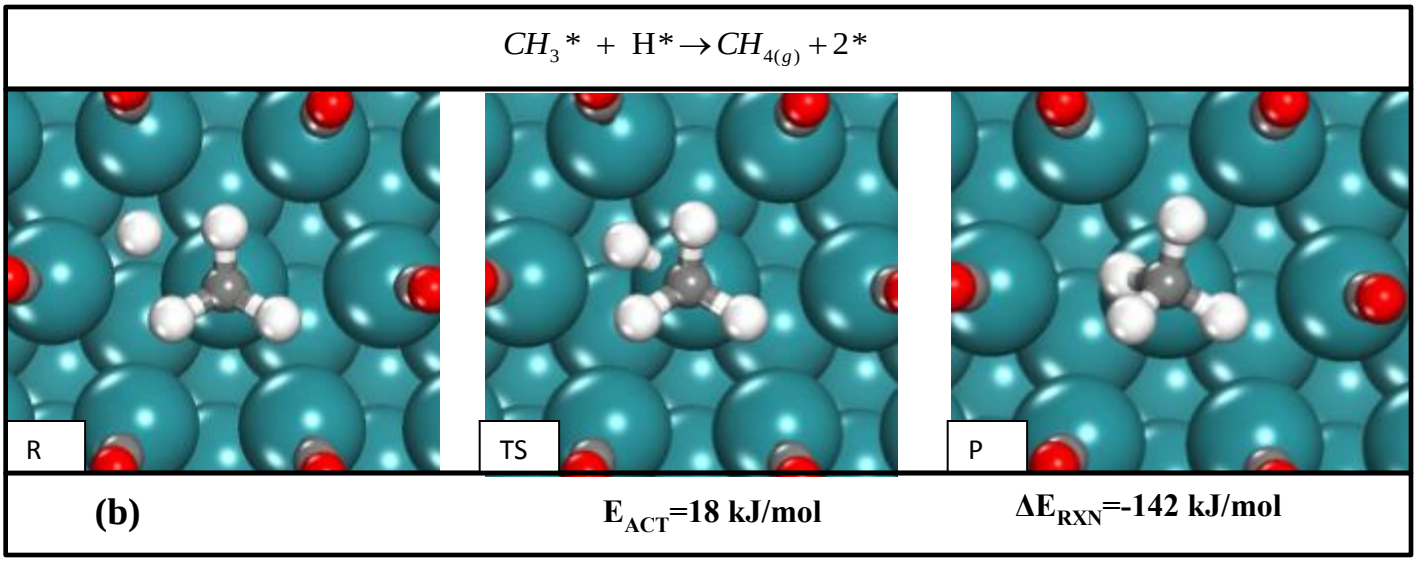

Figure 6: Reaction energies for CO insertion (a) and hydrogenation (b) of methyl (CH_3) on (111) terrace sites of Ru_{119} half particle at 1ML CO* coverage. Ru atoms are teal, oxygen atoms are red, carbon atoms are gray, hydrogen atoms are white.*

Reaction Energies for CO Insertion and Hydrogenation of CH_x Summarized*

The dominant chain propagation path for the CO insertion mechanism in FTS will be the one with the lowest overall free energy barrier up to the transition state of the first irreversible step along the particular path. The DFT calculated Gibb's free energy diagram which is shown in Figure 7 compares the free energy barriers and overall reaction free energies for all of the CO insertion and hydrogenation steps of CH_x*. The resting state of the catalyst is taken to be adsorbed methylidyne and $H_{2(g)}$, which is consistent with kinetic and infrared experiments and theory studies of the reaction on Ru and Co [6,8,9,10,17]. The reference state for this analysis thus represents a "snapshot" of the catalyst just after the initiation of C-O* to form methylidyne and which kicks off the chain growth reaction.

The free energy diagram in Figure 7 indicates that the most favorable C-C bond formation reaction involves the reaction of CH* with CO*. This is the result of both the moderate intrinsic activation barrier for the reaction (65 kJ mol^{-1}) along with the weak binding energy of H*. The latter makes the free energy for the chemisorption of $H_{2\,(g)}$ $\Delta G_{ads}(H_{2\,ads})$ slightly negative. As such the resulting thermodynamics indicate that surface coverage of H* is very low compared to the coverage of the strongly held CO*. The entropy losses associated with the chemisorption of hydrogen and the subsequent H* addition steps lead to the increasing free energy path where the CH_x* fragments "climb upwards" as shown in Figure (7).

The reaction coordinate diagram also indicates that the acyl intermediate (CH_3CO*) has a lower free energy value (26 kJ mol^{-1}) than that of both the CHCO* (53 kJ mol^{-1}) and CH_2CO* (54 kJ mol^{-1}) intermediates. This appears to be the result of balancing the endothermic hydrogenation steps and the exothermic alkyl migration/CO insertion step. The insertion of CO and the adsorbed alkylidyne and alkylidene intermediates, on the other-hand were all calculated to be endothermic. The exothermicity associated with the reactions of CO and CH_3* to form the CH_3CO* intermediate is associated with the enthalpic gains as well as the entropic relief that results in moving the CH_3* above the adlayer. This also avoids the entropy losses that would otherwise be incurred due to the loss in entropy associated with the removal of degrees of freedom associated with the consumption of hydrogenation. The favorable intrinsic energetics of the alkyl CO Insertion reaction ultimately makes the formation of CH_3CO* more favorable than the formation of either CHCO* and CH_2CO*

In what follows, we examine the activation of the C-O bond of the CH_xC-O * intermediates formed by the initial CO insertion into the Ru-CH_x bond in order to determine the lowest free energy reaction path for chain propagation via the CO insertion mechanism which includes the different C-C bond formation steps via CO insertion, CH_x* hydrogenation steps and the irreversible C-O bond activation.

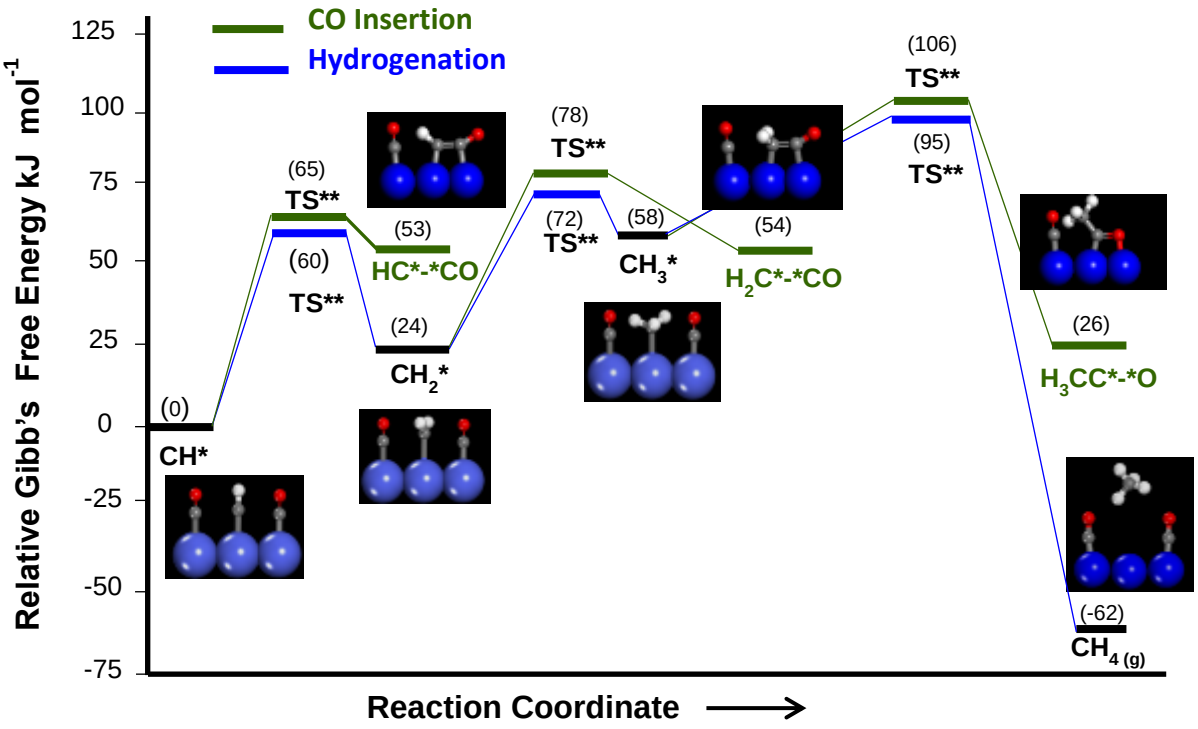

*Figure 7. Free energy comparison of CO insertion and hydrogenation of CH_x *. All energies in kJ mol^{-1} and relative to adsorbed methylidyne at 1 ML CO* coverage and $H_{2\,(g)}$, T=463 K.*

CO Insertion Chain Propagation and C-O Activation via Alkylidyne Pathways

Once the CHCO* intermediate is formed the C-O bond can be activated. We explored both the direct and H*-assisted C-O activation mechanisms to dissociate the CHCO*. The H-assisted

paths examined explored the addition of a single hydrogen to the oxygen atom of CHCO*. This path is analogous to previous theoretical results that showed that RC-O* is readily activated via H* additions to the oxygen atom [6,8,9,10]. The results shown in Figure 8 indicate that the direct activation of CHC-O* is rather difficult as the calculated barrier is over 137 kJ mol^{-1}. This reaction proceeds by the initial elongation of the C_α-O bond. The C-O π bond is nearly fully cleaved in the transition state as the distance between the Cα and the O atom is 1.92 Å where the oxygen atom has formed two Ru-O bonds with the surface (averaging 2.04 Å). The C-C bond of HCC* has a distance typical of C-C π bonds of 1.38 Å. The CH group of CHC* forms a single Ru-C bond at 2.20 Å, one C-H bond (1.10 Å) and a single C-C π bond with a distance of 1.38 Å while the other C atom sits in a threefold site. This step has a high energy barrier for this reaction E_A =137 kJ $mol^{-}1$. Overall the reaction is exothermic , ΔE_{RXN} =-30 kJ mol^{-1}.

The activation of the C-O bond of CHCO* can also proceed via a hydrogen-assisted route where hydrogen first adds to the oxygen of CHCO*. This weakens the C-O bond and thus enables C-O scission via the path shown in Figure (8 b and 8-c). The reaction proceeds by the migration of hydrogen towards the oxygen atom. This results in a moderately high intrinsic barrier for the reaction E_a=77 kJ mol^{-1}. The O-H bond distance in the transition state is 1.51 Å. The product of this step is CHCOH* which is more stable than the reactant (CHCO* + H*) state. This reaction appears to be exothermic with a reaction energy of ΔE_{RXN} =-65 kJ mol^{-1}. Figure (8 c) below shows that the scission of the C-O bond of CHCOH* proceeds via a hydrogen addition to the oxygen atom of CHCO*. This reaction proceeds via elongation of the C-O bond of the CHC-OH* intermediate. In the transition state, the C-O bond appears to be fully broken where the distance between the oxygen atom and the α carbon is 1.95 Å. The oxygen atom of the hydroxyl surface intermediate forms a bond with a neighboring Ru atom on the terrace of 2.18 Å in the

transition state. This step has a high activation barrier to proceed E_a=157 kJ mol^{-1}. This step is exothermic and ΔE_{RXN} =-35 kJ mol^{-1}.

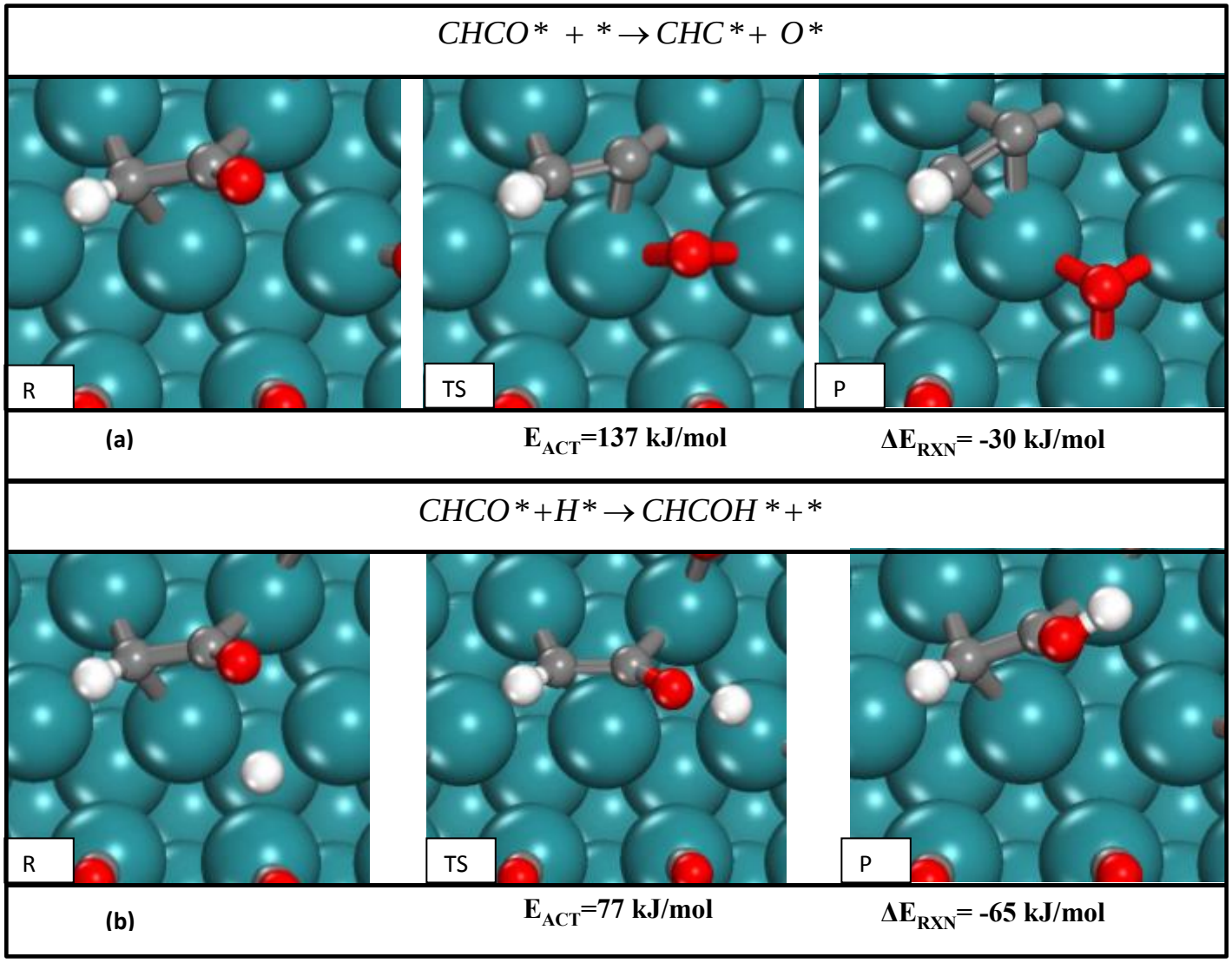

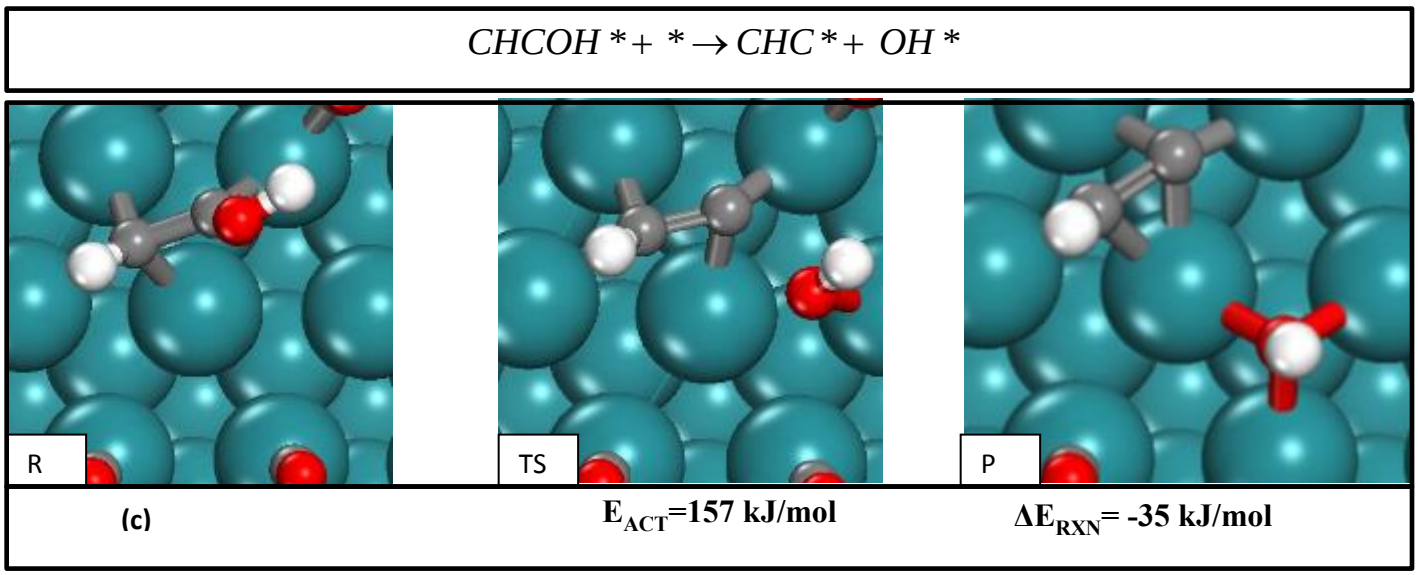

Figure 8: Direct and H-assisted activation of CHCO on the (111) terrace sites of Ru_{119} half particle at 1ML CO* coverage. (a) CO scission of CHC-O* (b) H* addition to CHCO* (c) CO scission of HCC-OH*.*

Summary of the Propagation Path which Proceeds via CO Insertion into Surface Alkylidyne Intermediates.*

The energetics for chain propagation paths which proceed via the insertion of CO* into the Ru-alkylidyne intermediates followed by the activation of the C-O bond are summarized in the free energy diagram shown below in Figure (9) which shows that the path involving the direct activation of the C-O bond has a free energy barrier of 190 kJ mol^{-1} relative to adsorbed methylidyne. The H* assisted CHCO* activation path, however, has a free energy barrier of 152 kJ mol^{-1} relative to adsorbed methylidyne and the CHCOH* intermediate. It is an exothermic reaction with a free energy of reaction of -22 kJ mol^{-1} relative to the reference state. The next step, involves the C-O scission of the CHCOH* intermediate. This step has the highest barrier taken with respect to the adsorbed methylidyne of the two steps involved in the H-assisted activation pathway with a barrier of 167 kJ mol^{-1}. Thus the preferred chain growth reaction path for the alkylidyne intermediate involves the CO insertion into the metal-CH* bond followed by H* assisted

activation of the resulting CHCO* intermediate by the addition of H* to the oxygen atom. This chain growth path has an effective Gibb's free energy barrier for chain growth of 167 kJ mol^{-1} taken with respect to adsorbed methylidyne. and $H_{2(g)}$.

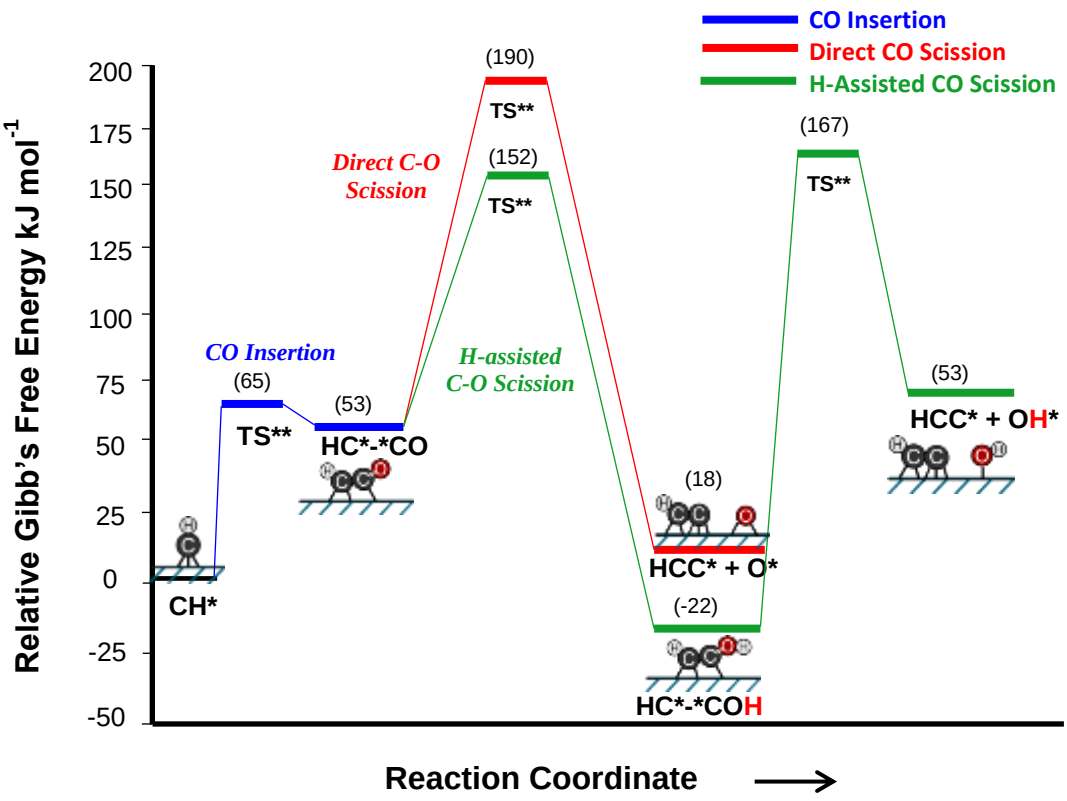

Figure 9: Free energy diagram for C-C bond formation and chain growth via the presence and reactivity of alkylidyne intermediates. CO insertion is followed by C-O activation via the \direct and H-assisted paths. Energy values in kJ mol^{-1}, T=463 K.

CO Insertion Propagation via Alkylidene Pathways

In what follows, the same sequence of C-C formation and C-O bond activation steps taken for the alkylidyne path occur here for the alkylidene route. It was previously noted in Figure (7) above that the CH_2CO* intermediate that forms via CO insertion with methylidene has a free energy of 54 kJ mol^{-1} relative to adsorbed methylidyne. Once the CH_2CO* intermediate is

formed it can undergo direct C-O activation on the surface or proceed via the H* addition to the RC-O* bond. Figure (10-a) below shows the direct activation of CH_2CO^* to form $CH_2C^* + O^*$. The intrinsic barrier for direct metal catalyzed C-O bond activation is high at E_a=130 kJ mol^{-1} again showing that direct activation of the C-O bond is a difficult step. In the transition state of this reaction the C-O bond is fully cleaved and the distance between O* and the α C* is 1.83 Å. The oxygen atom that dissociates from the CH_2C^* sits in a bridge site between two Ru atoms on the terrace with bond lengths averaging 2.02 Å. The products for this step are O*, which sits in a threefold hollow site on the terrace, and CH_2C^*, and CH_2C^* which preferentially binds to the unsaturated carbon in a threefold hollow site and has a C-C bond length of 1.38 Å. DFT results indicate that this step is exothermic , ΔE_{RXN} =-30 kJ mol^{-1}. The H-assisted activation of the C-O bond occurs by H* addition the O atom. This step which is shown in Figure (10 b) has an intrinsic barrier of E_a=99 kJ mol^{-1}. A significant portion of the barrier for this reaction results from the scission of the strong Ru-O bond (of 2.09 Å) that helps to anchor the reactive intermediate CH_2CO^* to surface. The Ru-O bond elongates to 2.13 Å in the transition state and the distance between hydrogen and the oxygen atom is 1.37 Å. The Ru-O bond is fully ruptured in the product state and the O-H bond (with length of 0.98 Å) is fully formed. This step is endothermic with ΔE_{RXN} =23 kJ mol^{-1}. The subsequent scission of the C-O bond for the bound CH_2OH intermediate is shown in Figure (10-c). The activation barrier for C-O scission step is E_a=48 kJ mol^{-1} which is significantly lower than that for the C-O scission without hydrogen addition. The addition of hydrogen transfers electrons into the π-antibonding states of C-O thus facilitating its rupture. This reaction is exothermic with ΔE_{RXN} =-14 kJ mol^{-1}.

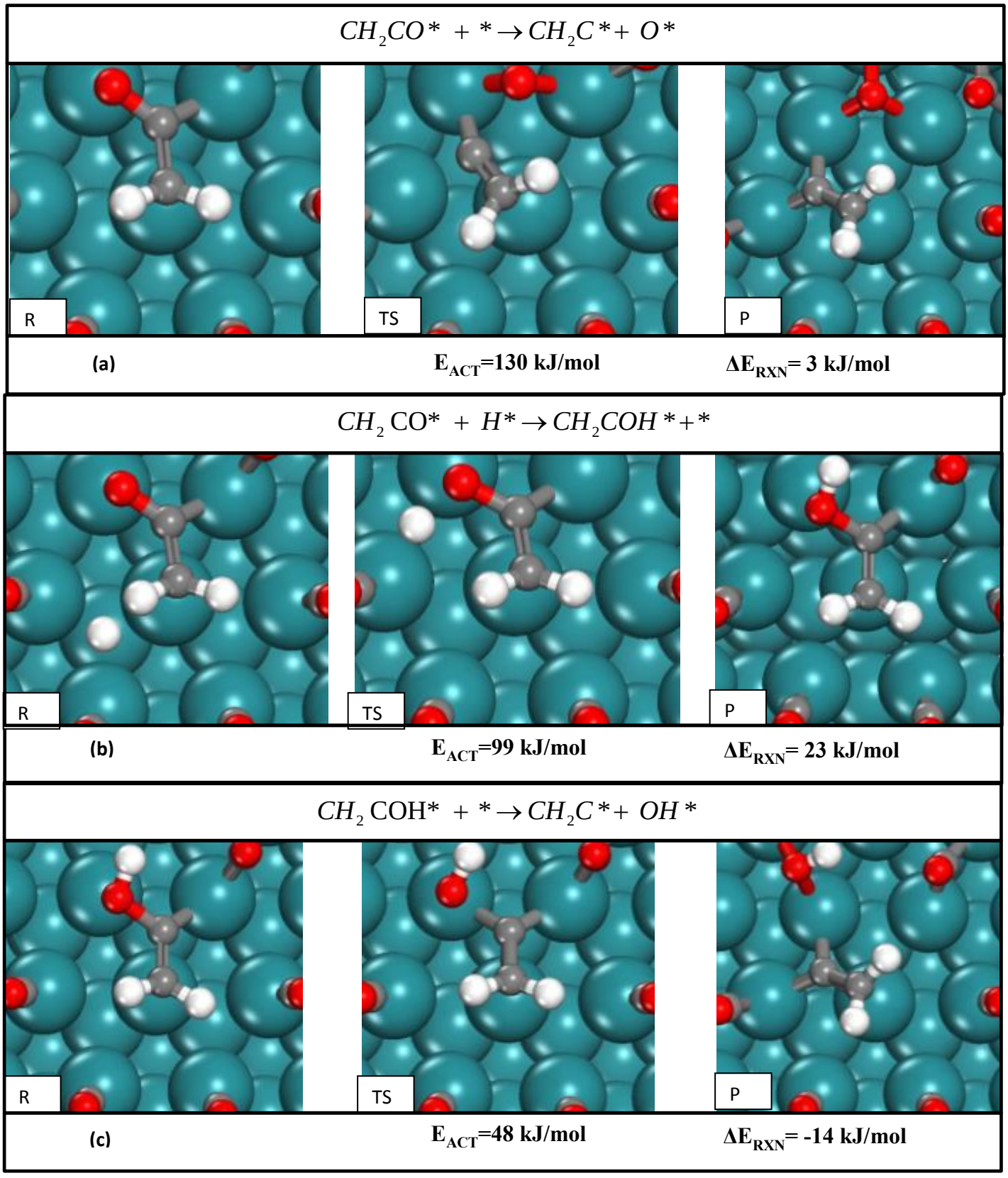

Figure 10: Direct and H-assisted activation of CH_2 CO on (111) terrace sites of Ru_{119} half particle at 1ML CO* coverage. (a) CO scission of CH_2 C-O* (b) H* addition to CH_2 CO* (c) CO scission of H_2 CC-OH*.*

Summary CO Insertion Propagation via Alkylidene Pathways

The chain propagation steps for the CO reactions with adsorbed alkylidene intermediates followed by the C-O bond scission steps involved in the alkylidene propagation paths are summarized in the free energy diagram shown below in Figure (11). This diagram shows that the chain growth path involving the direct activation of the C-O bond has a free energy barrier of 184 kJ mol^{-1} relative to adsorbed methylidyne and $H_{2\,(g)}$. The H-assisted C-O scission paths are also reported in Figure 11. The hydrogen addition path has a barrier of 163 kJ mol^{-1} relative to adsorbed methylidyne which is significantly lower than the direct C-O scission path (84 kJ mol-1) but only slightly lower than the path through the alkylidyne intermediate (*HC-COH*) 167 kJ mol^{-1} shown back in Figure (9).

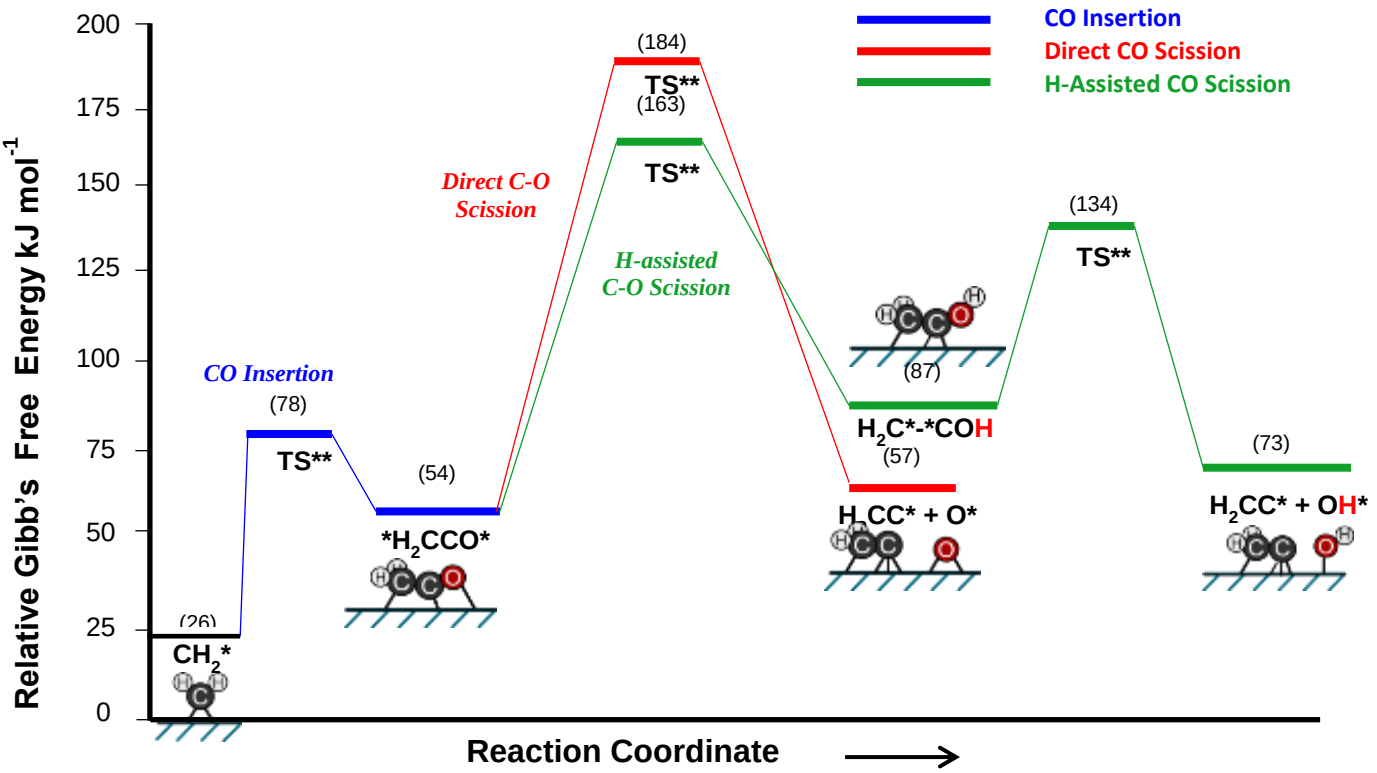

Figure 11: Free energy diagram for the chain growth via CO addition reactions with the alkylidene intermediate. CO insertion followed by C-O activation via the direct and H-assisted pathways. Energy values in kJ mol^{-1}, T=463 K.

CO Insertion Propagation via Alkyl Pathways

Next, the sequence of elementary steps for chain propagation via the alkyl CO insertion mechanism for $C_1^* \rightarrow C_2^*$ as well as the formation of acetaldehyde and possible C-O bond dissociation of the adsorbed aldehyde were investigated. Figure (12 a) below shows the direct C-O activation of the adsorbed acyl (CH_3CO^*) formed via the addition of CO* to CH_3*.The activation barrier for the direct dissociation of CH_3CO^* to form CH_3C^* and O* was calculated to be 123 kJ mol^{-1} which is high compared to the H*-assisted paths discussed below. The overall

reaction energy for this step was calculated to be -30 kJ mol^{-1}. The H* assisted activation of the acyl proceeds via the addition of H* to the O of the bound CH_3CO* as is shown in Figure (12 b). The Ru-O bond of the acyl is nearly fully ruptured in the transition state as the distance between O* and the nearest Ru atom is 2.41 Å . The activation barrier for this step is 99 kJ mol^{-1} where a significant fraction of the energy cost comes from breaking the strong Ru-O bond. This step is endothermic at 49 kJ mol^{-1} and results in the formation of the hydroxyethylidene (CH_3COH*) intermediate. The CH_3COH* intermediates is activated by the electron transfer that occurs upon the addition of H* and thus rapidly undergoes C-O scission, shown in Figure (12 c) with an activation barrier of only 32 kJ mol^{-1}. This step is rather exothermic and irreversible with ΔE_{RXN} =-69 kJ mol^{-1}.

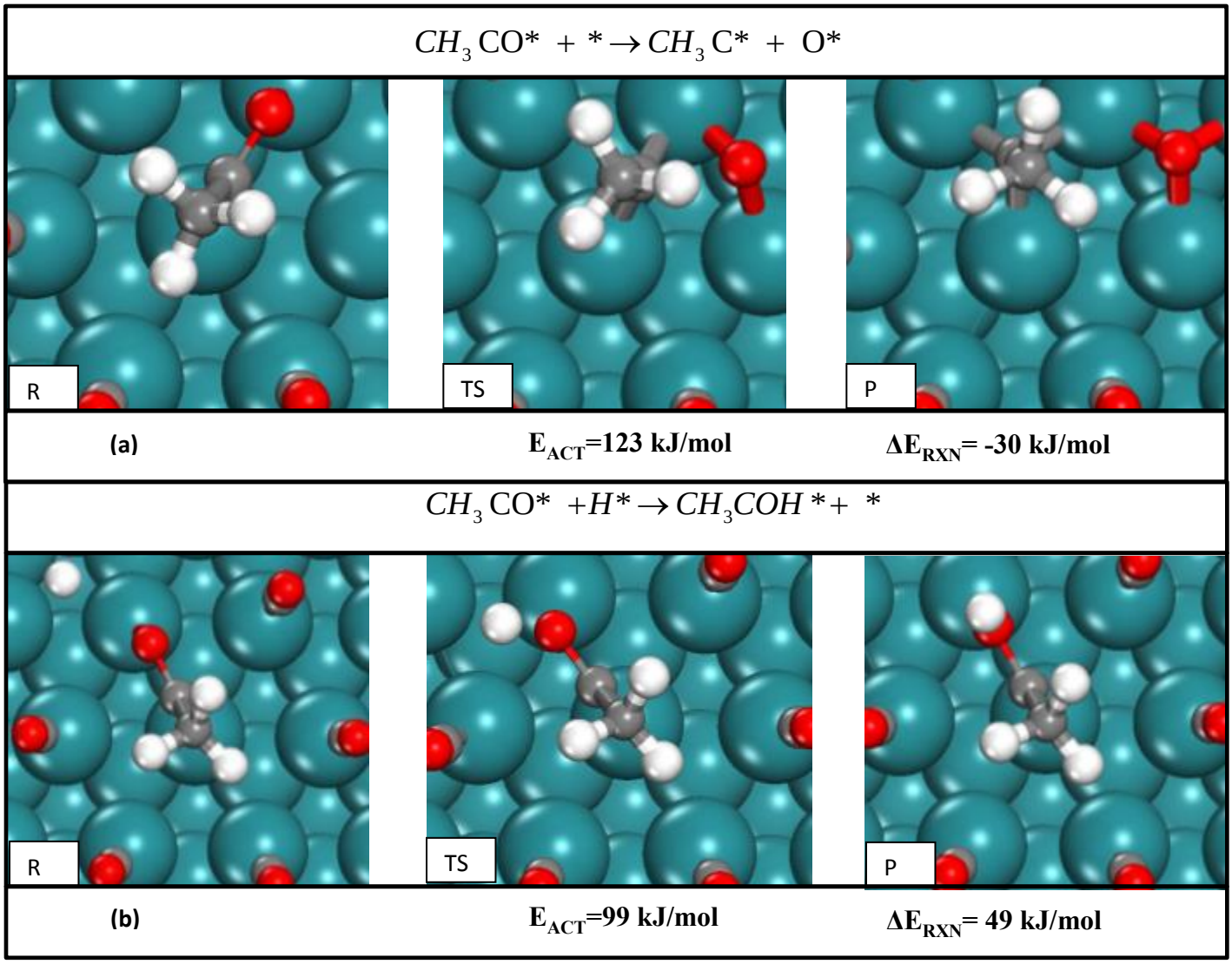

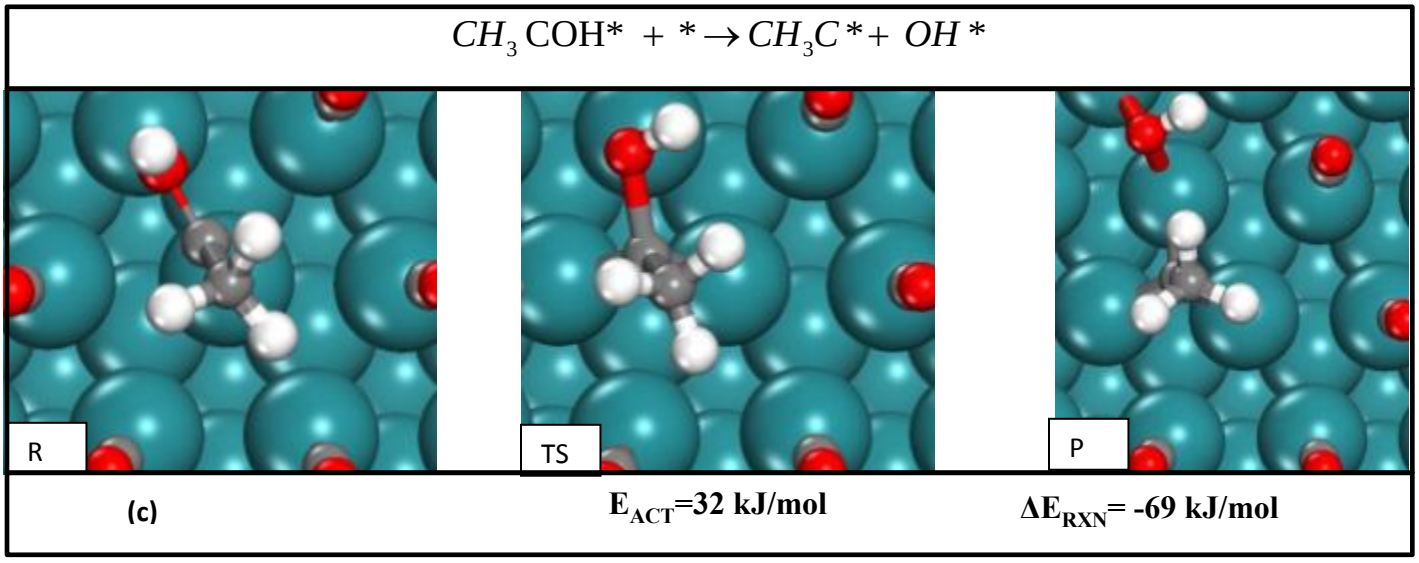

Figure 12: Direct and H-assisted activation of CH_3 CO on (111) terrace sites of Ru_{119} half particle at 1ML CO* coverage. (a) CO scission of CH_3 C-O* (b) H* addition to CH_3 CO* (c) CO scission of H_3CC-OH*.*

Alternatively, hydrogen can add to the α carbon with a relatively low calculated activation barrier of 68 kJ mol^{-1} to form adsorbed acetaldehyde as shown in Figure (13 a). The acetaldehyde product prefers to bind to Ru in an η_1 -C η_2-O configuration as shown in Figure (13 a). This path was investigated since oxygenate production in FTS is rather low as compared to n-alkane and 1-alkene production. While H* addition to the carbon atom of an acyl is an easier step it does not significantly alter the strength of the C-O bond or aid in direct C-O scission. This can be seen in Figure (13 b) which shows a high barrier for the direct C-O scission of (CH_3CHO*), E_a=103 kJ mol^{-1}. This reaction is with an overall energy of ΔE_{RXN} =-23 kJ mol^{-1}.

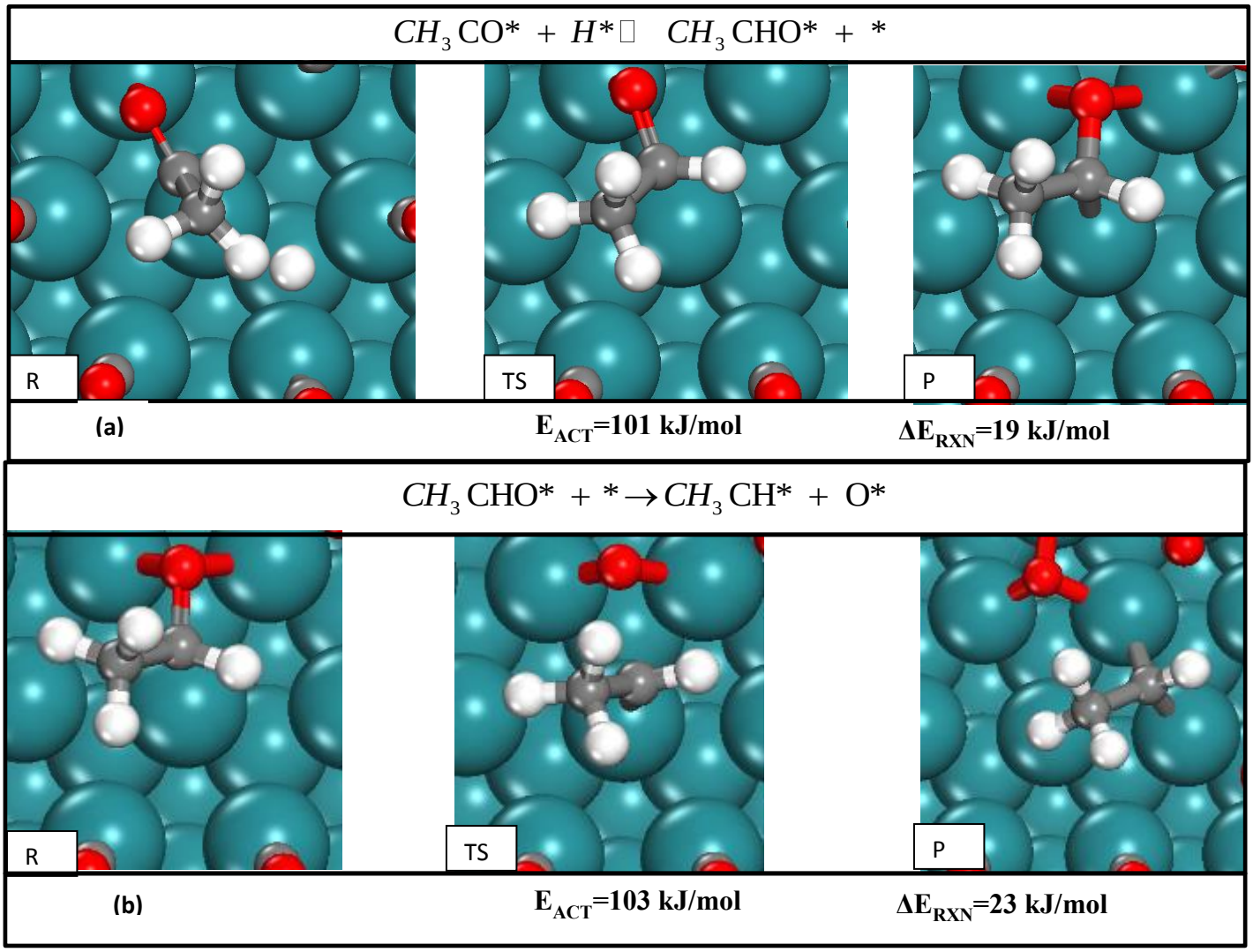

Figure 13: (a) H- addition to acyl to form adsorbed acetaldehyde (CH_3 CHO*) (b) C-O scission of acetaldehyde to form ethylidyne (CH_3 CH*) and O*.*

Summary of CO Insertion Propagation via Alkyl Pathways

Chain propagation via CO insertion with alkyl intermediates followed by the activation of the C-O bond are summarized in the free energy diagrams shown below in Figures (14) and (15) .The pathway involving direct activation of the C-O bond which is shown in Figure (14) has a free energy barrier of 149 kJ mol^{-1} relative to adsorbed methylidyne. This pathway is lower than those involving the alkylidyne (167 kJ mol^{-1}) and alkylidene (163 kJ mol^{-1}) intermediates which were investigated and discussed above.

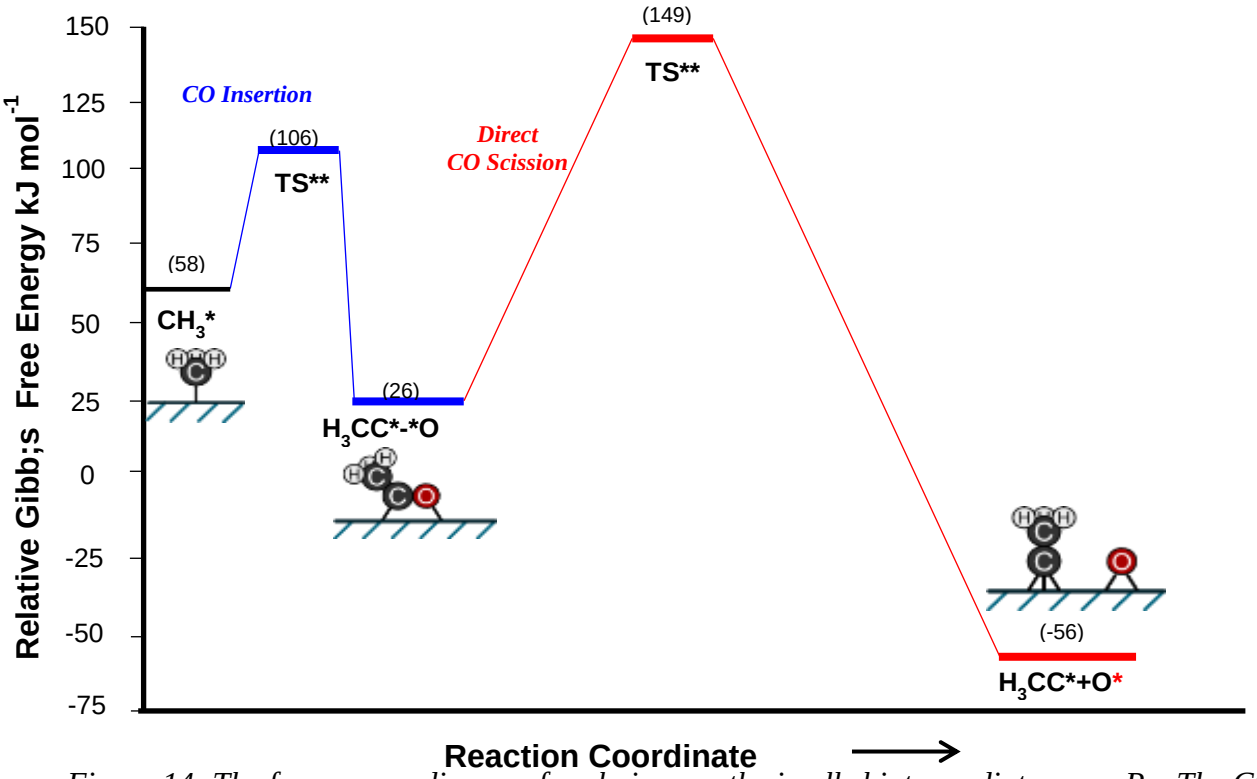

Figure 14: The free energy diagram for chain growth via alkyl intermediates over Ru. The CO inserts into the Ru-CH_3 to form an acyl intermediate which undergoes C-O activation. Energy values in kJ mol^{-1}, T=463 K.

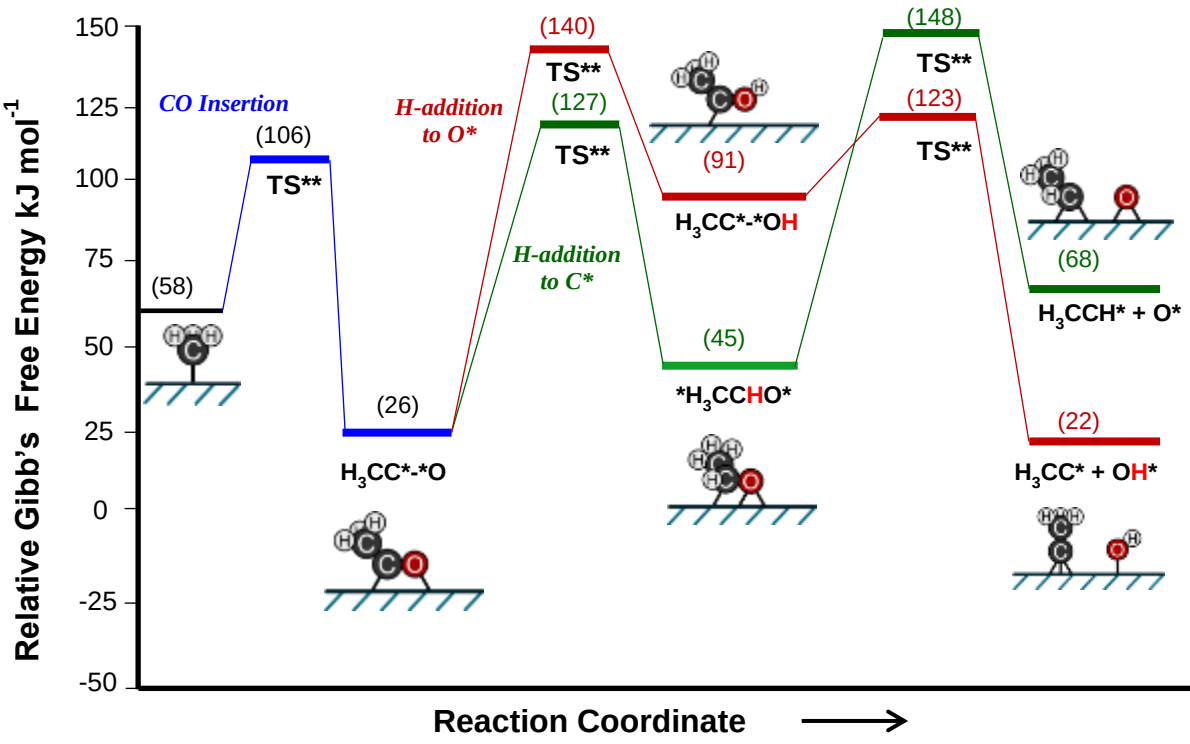

Figure 15: Free energy diagram for the chain growth via alkyl intermediates. CO insertion is followed by H-assisted activation of the acyl intermediate. There is a direct comparison of the paths involving H* addition to C* and O*. Energy values in kJ mol^{-1}, T=463 K.*

Figure (15) shows results associated with H adding first to the O* of RC-O* . The reaction energies and transition states calculated indicate that it easy to form acetaldehyde which has a modest intrinsic energy barrier and a free energy of 127 kJ mol^{-1} relative to adsorbed methylidyne. The activation of the C-O bond of the resulting aldehyde however is somewhat higher with a free energy of 148 kJ mol^{-1} to form the *CH_3CH--O* intermediate. On the other hand, while the H* addition to the oxygen atom CH_3CO* is initially more difficult, (relative free energy value of 140 kJ mol^{-1}) it ultimately is the more favored propagation pathway to the activation of RC-O*. Consequently, it may be expected that any aldehydes formed would be quasi-equilibrated and undergo a reversible dehydrogenation step, oscillating between a surface acyl intermediate and a bound aldehyde, until either the aldehyde desorbs from the surface or H* is added to O* of the intermediate in an irreversible propagation step.

C-C Bond Formation via CH_x-Insertion

The second major route to carbon-carbon bond formation involves the coupling of surface CH_x intermediates via the CH_x insertion mechanism. For CH_x insertion with (x=1,2,3) there are 6 possibilities for the coupling of C_1* to form C_2* intermediates (9 for C_n* $\longrightarrow$ C_{n+1}* where n > 1). The results from these reaction pathways are summarized below in Table 2. In all of the cases for C-C coupling via CH_x insertion, the calculated reaction energies range from being moderately exothermic to highly exothermic.

Table 2: The activation energies and overall reaction energies for CH_x insertion mechanism (x= 1-3) on (111) terrace sites of Ru_{119} half particle at 1ML CO coverage all values reported in kJ mol^{-1}*

Reaction	E_A	ΔE_{RXN}
$CH^* + CH^* \longrightarrow CHCH^* + *$	67	-33
$CH^* + CH_2^* \longrightarrow CHCH_2^* + *$	42	-52
$CH^* + CH_3^* \longrightarrow CHCH_3^* + *$	39	-57
$CH_2^* + CH_2^* \longrightarrow CH_2CH_2^* + *$	34	-95
$CH_2^* + CH_3^* \longrightarrow CH_2CH_3^* + *$	41	-97
$CH_3^* + CH_3^* \longrightarrow C_2H_{6\,(g)} + 2^*$	109	-224

The reactant, transition and product state structures for the reaction in Table 2 are shown in Figures (16 a-f) for the C-C coupling reactions of C_1 to form C_2 via CH_x insertion mechanisms.

The reaction between two alkylidyne species to form the CH-CH* product is shown below in Figure (16). In the transition state one of the Ru-C bonds of methylidyne is ruptured as it migrates toward a vicinally bound methylidyne (CH*) to initiate chain growth. The calculation indicate that the reaction is exothermic with an overall energy of ΔE_{RXN} =-33 kJ mol^{-1}. The alkylidyne product was found to have a C-C bond length of 1.42 Å.

The different combinations of adding alkylidyne and alkylidene intermediates on the surface are shown in Figure (16-b). The transition state involved in the coupling of CH* and CH_2* involves the activation of the R-methylidene (CH_2*) bond as CH* migrates toward the CH_2*. This is effectively the barrier for CH_2* diffusion on a CO* covered terrace and has an activation barrier of 42 kJ mol^{-1}. This lower barrier is likely due to the fact that CH_2* forms fewer bonds to the surface and is bound more weakly than CH* (BE 330 kJ mol^{-1} < 546 kJ mol^{-1}) The reaction is exothermic and results in the formation of a *HC-CH_2* intermediate with ΔE_{RXN} =-52 kJ mol^{-1} and a C-C bond distance of 1.41 Å.

The surface alkylidyne can also react with surface alkyl intermediates. This path which is shown in Figure (16-c) involves the migration of the alkyl group toward the alkylidyne (CH*), the insertion of the alkyl into the Ru-CH* bond, the formation of the C-C bond and the rupture of the Ru-C bonds of the alkyl (CH_3*). The activation barrier for this step is rather low at 39 kJ mol^{-1}. The low barrier is the result of the weak binding of CH_3 due to its significant repulsion with the dense CO* adlayer. The formation the *HC-CH_3* intermediate is exothermic with ΔE_{RXN} =-57 kJ mol^{-1}

In moving to the reactions of methylidene, two methylidene species can react to form ethylene as shown in Figure (16-d). The reaction proceeds via the insertion of one of the methylidenes into the Ru-CH_2 bond of the second methylidene along with the formation of the C-C bond. In the transition state one of the Ru-C bonds of CH_2* is completely ruptured. The low activation barrier of 34 kJ mol^{-1} that was calculated is again likely the result of the repulsive interactions of the CH_2* groups with the dense CO* adlayer. The reaction is exothermic and results in the formation of a *H_2C-CH_2* intermediate with an overall reaction energy of ΔE_{RXN} =-95 kJ mol^{-1} and a C-C bond distance of 1.40 Å.

The surface methylidene intermediate can also react with a bound alkyl intermediate as is shown in Figure (16-e) for the C-C bond formation between CH_2* and CH_3*. The reaction proceeds via the migration of the methyl intermediate along the Ru surface, its insertion into the Ru-CH_2* bond, the formation of the C-C bond and the full rupture of the Ru-alkyl bond. The low barrier of 34 kJ mol^{-1} is again likely the result of the weak Ru-CH_3* that results from its repulsive interactions from the dense CO adlayer. This reaction to form the surface ethylene was calculated to be exothermic where ΔE_{RXN} =-95 kJ mol^{-1} and a C-C bond distance of 1.40 Å.

The final CH_x coupling path involves the coupling of two surface alkyl intermediates as is shown in Figure (16-f). This reaction leads to termination of the chain via the production of the alkane (ethane) product. In the transition state both the Ru-C bonds of the methyl groups are ruptured. The CH_3* groups are quite bulky and do not like to approach each other on the surface. As such the activation barrier is rather high (109 kJ mol^{-1}) compared to the other CH_x coupling paths. The reaction is highly exothermic clearly showing that the termination to n-alkanes in FTS is irreversible and results in the formation of desorbed ethane ΔE_{RXN} =-224 kJ mol^{-1} and a C-C bond distance of 1.52 Å.

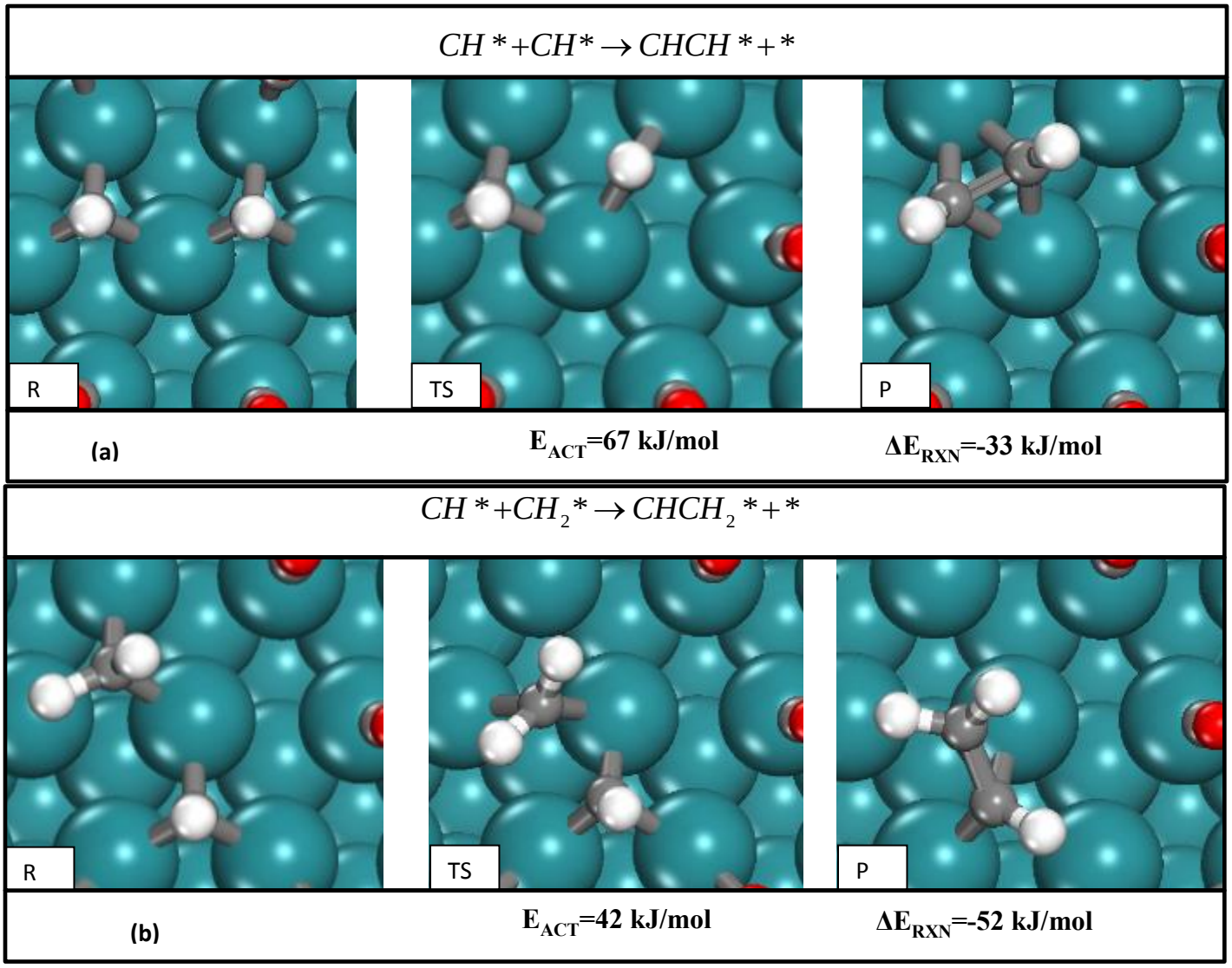

$$CH^{*}+CH_3^{*}\rightarrow CHCH_3^{**}$$

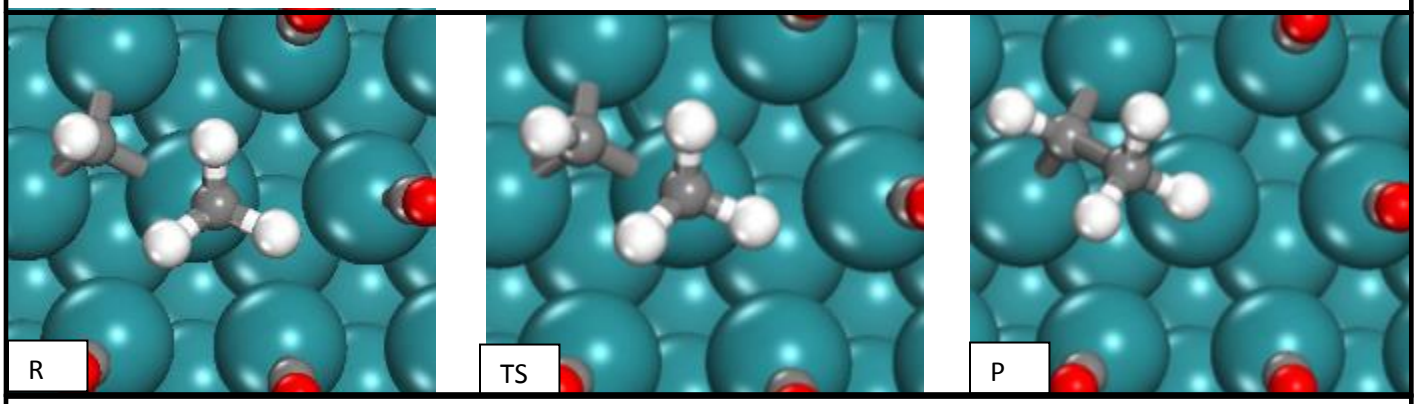

(c) E_{ACT}=39 kJ/mol ΔE_{RXN}=-57 kJ/mol

$$CH_2^{*}+CH_2^{*}\rightarrow CH_2CH_2^{**}$$

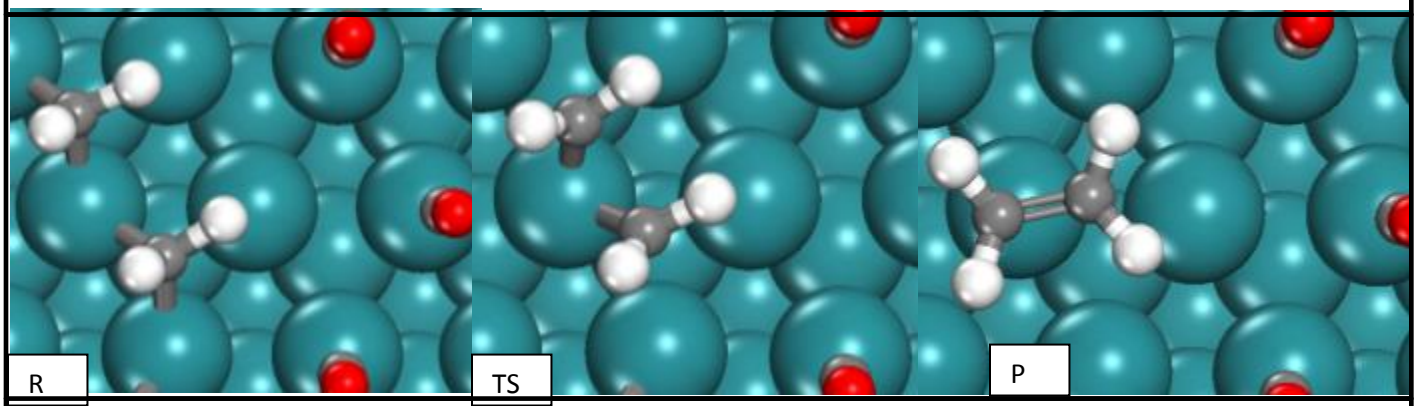

(d) E_{ACT}=34 kJ/mol ΔE_{RXN}=-95 kJ/mol

$$CH_2^{*}+CH_3^{*}\rightarrow CH_2CH_3^{**}$$

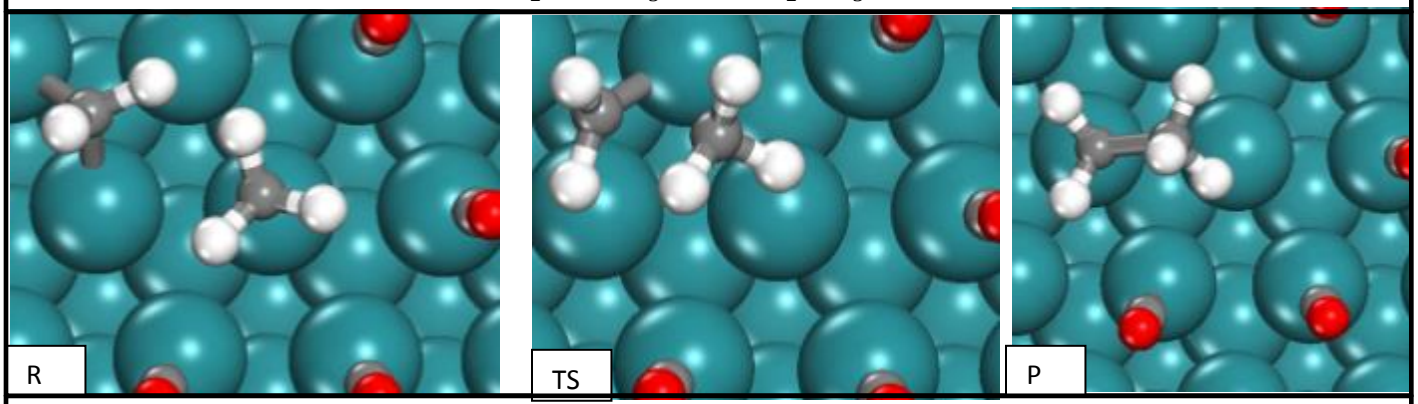

(e) E_{ACT}=41 kJ/mol ΔE_{RXN}=-97 kJ/mol

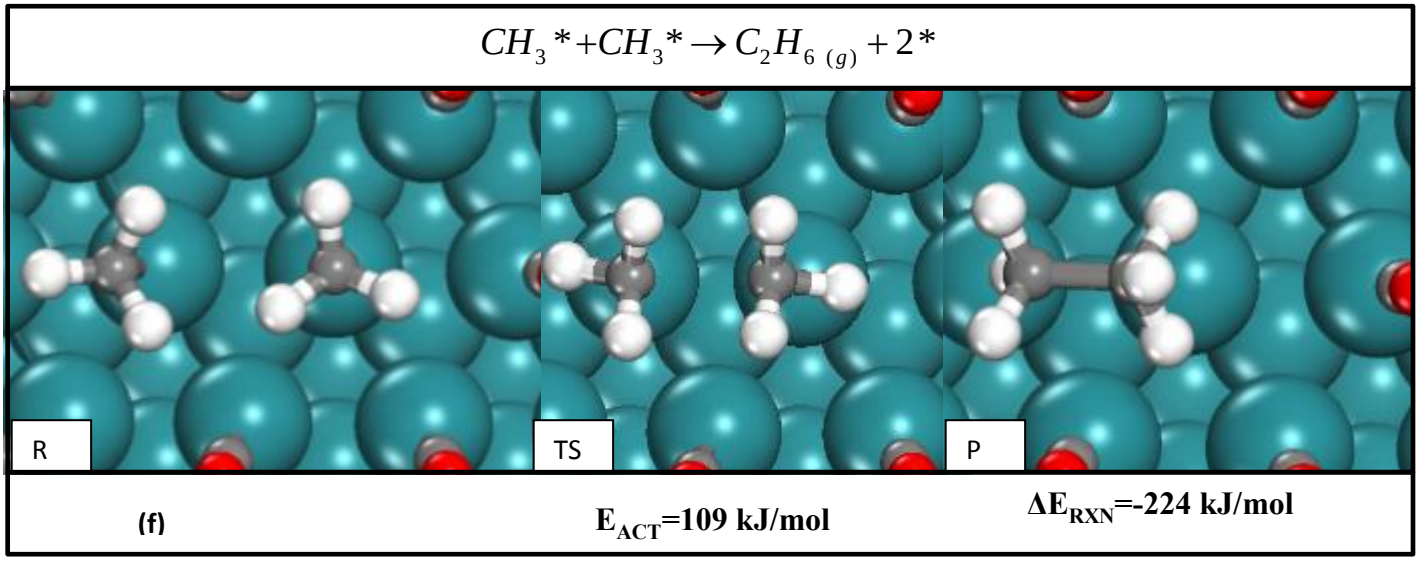

Figure 16: Carbon-carbon coupling via CH_x insertion at high CO coverages on Ru resulting in the formation of: (a) HC-CH (b) HC-CH_2 (c) HC-CH_3 (d) H_2C- CH_2 (e) H_2C- CH_3 (f) H_3C- CH_3.*

.

Summary of C-C Bond Formation Reactions via CH_x-Insertion

A comparison of all of the free energy barriers and overall free energies for the C-C bond forming paths examined herein is shown in Figure (17). All the energies are plotted relative to the free energy for two infinitely separated CH* intermediates and $H_{2\ (g)}$. The results clearly show that intrinsic activation energies increase with increasing the degree of hydrogen within the surface CH_x* intermediate. This is due, in part, to the fact that the ΔG_{ads} for H* addition is positive as a result of the weak binding energy of H* (and hence low ΔH_{ads}) and high entropy losses associated with the chemisorption of $H_{2\ (g)}$. Inspection of the free energy diagram reveals that the lowest C-C bond formation transition states via CH_x insertion are the result of the combination of two surface alkylidyne species (CH* + CH*) as well as the combination of an alkylidyne with an alkylidene (CH* + CH_2*) which proceed with nearly identical calculated relative Gibb's free energy barriers of 67 and 68 kJ mol^{-1} respectively. The results suggest that

entropy penalties for H* additions make the free energies of kinetically relevant (H_xC-CH_y) C-C bond forming transition states unfavorable when analyzed from the perspective of the resting state of the catalyst (CO*) ~ 1, $H_{2(g)}$ at the relevant conditions of temperature and pressures typical of FTS practice.

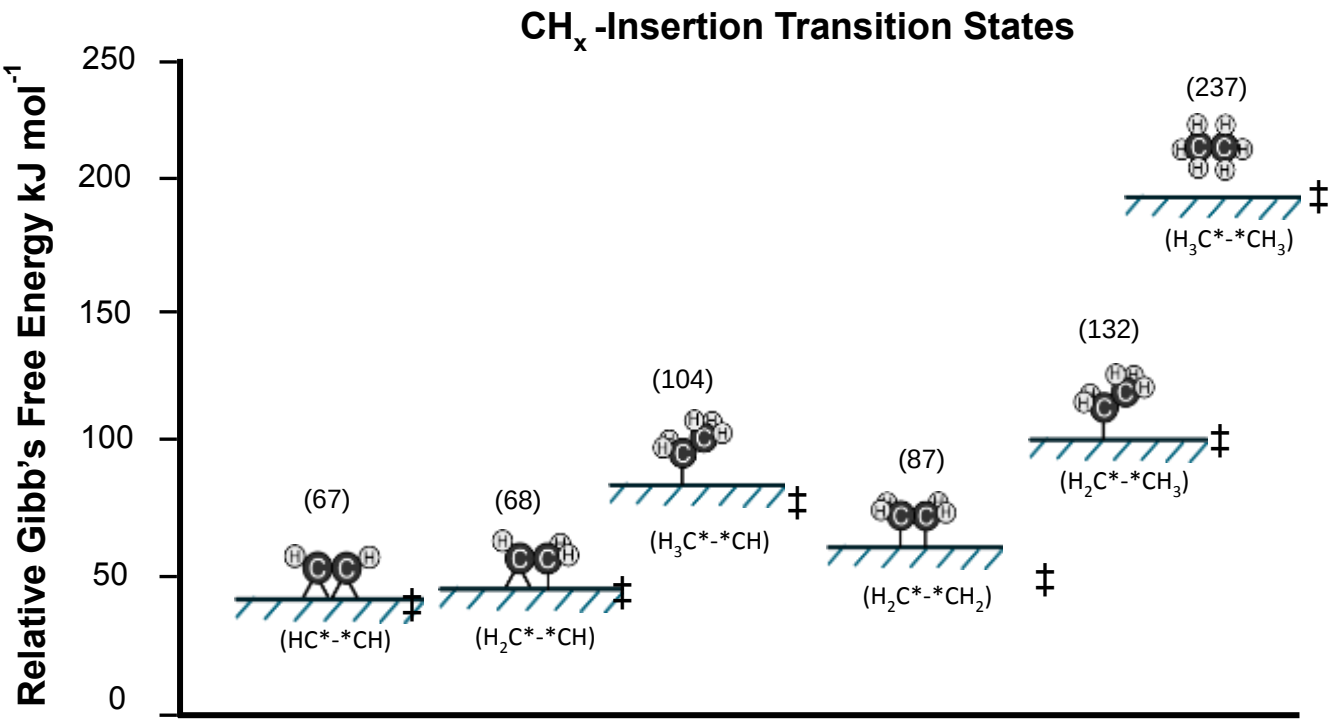

Figure 17: A comparison of the free energy barriers and overall reaction energies for all of the C_{1Hx}-C_{1Hy} bond formation steps that can occur on the surface of the Ru clusters. All energies relative to (CH + CH*) infinitely separated on CO* covered particle and $H_{2\,(g)}$, T=463 K.*

Discussion

A number of different plausible C-C bond formation paths involving the reactions of C_1* monomers to form C_2* intermediates via both CO insertion and CH_x coupling chain growth mechanisms have been investigated on low index (111) terraces of Ru particles at high CO* coverages in the work carried out herein. DFT-calculated Gibb's free energy diagrams indicate that chain growth will take place via the H* assisted activation of surface acyl intermediates. H* addition to the oxygen atom CH_3CO* results in electron transfer into antibonding states of the CO that weaken the C-O in forming the hydroxyethylene transition state. This is an irreversible step that enables the direct scission of the C-O bond to form CH* and OH* surface intermediates.

The calculation results indicate that two hydrogen addition steps are required to form the surface methyl intermediate from methylidyne. These steps are likely reversible and may be considered quasi-equilibrated. The two H* addition steps are thought to be followed by the subsequent CO insertion into CH_3*. The C-O bond activation is thought to be controlled via the addition of surface H* to the oxygen atom of CH_3CO* to form the CH_3COH* intermediate. The H* assisted activation of CH_3CO* appears to be irreversible and thus it completes the propagation cycle. The elementary step kinetics (given in The Appendix) can be used to derive the chain growth probability α_n and chain termination parameter β_n given below

$$\alpha_n\left(\mathrm{T},\mathrm{P}_{CO}\mathrm{P}_{H_2}\right)=\frac{1}{(1+\beta_n)}=\frac{k_{act}K_{C-C}\,\mathrm{K}_{CO}\,K_{H_2}^{1/2}\,\mathrm{P}_{CO}\,P_{H_2}^{1/2}}{k_{act}K_{C-C}\,\mathrm{K}_{CO}\,K_{H_2}^{1/2}\,\mathrm{P}_{CO}\,P_{H_2}^{1/2}+(k_tK_{H_2}^{1/2}P_{H_2}^{1/2}+k_o)}$$

Careful measurements of the chain termination parameter β_n and it's functional dependence on partial pressures of CO and H_2 can be used in conjunction with theoretical treatments to establish the accuracy and the likelihood of the proposed models and provide molecular insights into a non-trivial surface polymerization reaction.

SSITKA experiments carried out by Mims and McCandlish have shown that the chains that form on the surfaces of Co particles under FTS conditions are few and well-dispersed but grow very rapidly. They have growth rates that are much faster than the time required to replace the monomer pool from $^{12}C_1$* to $^{13}C_1$* [42]. This is consistent with the CO insertion mechanism as the CO* monomer is also the most abundant surface intermediate (MASI) and thus readily available for rapid chain growth [6,8,9,10].

The low intrinsic barriers calculated herein for C-C bond formation via CH_x coupling however would also be consistent with the coupling of two alkylidynes or an alkylidyne and alkylidene species dominant in the carbene mechanism. This was suggested by Maitlis who examined C-C bond formation in homogenous systems in detail by co-feeding various vinyl probe species. He proposed that alkenyl intermediates would be favored to alkyl intermediates because they have lower energy barriers to C-C coupling with μ-CH_2 groups than alkyls [21]. While the barriers for CH_x* coupling are low, the likelihood of two CH_x* species finding one another on surfaces covered by CO* would be very low as they would need to diffuse through a densely packed CO adlayer.

Recent theoretical and experimental studies indicate that FTS chain growth may be autocatalytic [10] whereby the CH* species that form upon the activation of CO* can assist in activating a vicinal CO* to from vicinal CH_x* intermediates that can readily react to form C_2H_y* products.

The results indicate that surface CH* and RCH* intermediates that forms upon CO* or RCO* activation retain a "a vacancy" on Ru that can be used to aid in the activation of a vicinal CO*. Thus, catalyzing the chain growth reaction by facilitating the formation of the reactive CH* groups at vicinal sites within the dense CO* adlayer in a scheme that is consistent with the rapid chain growth process required for the FT reaction [10,42] and does not involve isolated CH_x* intermediates that have to diffuse long distances to find one another.

Future work should be focused on rigorously calculating adsorbate and transition state entropies accurate free energies for all of the steps considered herein. These results will provide a solid foundation for kinetic studies. Kinetic Monte Carlo simulations have proven to be valuable in unraveling the molecular pathways involved in detailed metal catalyzed reactions. These simulations would help to establish the steady state CH_x* coverage. These simulations can also incorporate the diffusion of these intermediates on the surface, and their ability to couple to form C_2*. versus the reaction kinetics for the reactions of CH_x* with CO* and CH_y*. This would help to provide a detailed comparison for the kinetics of CO* insertion and CH_x* coupling and which paths dominate at FTS conditions.

Acknowledgements

I would like to thank the following people and organizations who helped to support this work. The Department of Chemical Engineering at the University of Virginia, Professor Neurock and the entire Neurock Group, Eric Dybeck, Craig Plaisance, Corneliu Buda. Experimental collaborators David Hibbitts and Professor Iglesia at the University of California -Berkeley and BP, for funding through the XC^2 program.

References

(1) Storch, H.H.; Golumbic, N.; Anderson, R.B. The Fischer-Tropsch and Related Synthesis; John Wiley and Sons: New York, 1951.

(2) Anderson, R.B.; Kolbel, H.; Ralek, M. The Fischer-Tropsch Synthesis; Academic Press: New York 1984

(3) Steynberg, A.P.; Dry, M.E. Fischer-Tropsch Technology; Elsevier: Amsterdam, 2004; Vol. 152.

(4) Tijmensen, M.J.A; Faaij, A.P.C; Hamelinck, C.N.; van Hardeveld, M.R.M. Exploration of the Possibilities of Fischer Tropsch Liquids and Power via Biomass Gasification. Biomass and Bioenergy, 2002, 23, 129-152

(5) van Santen, R.A.; Markvoort, A.J.; Filot, I.A.W.; Ghouri, M.M.; Hensen,E.J.M.; Mechanism and microkinetics of the Fischer-Tropsch Reaction. Phys. Chem. CHem. Phys. 2013, 15, 17038-17063

(6) Ojeda, M.; Nabar, R.; Nilekar, A.U.; Ishikawa, A.; Mavrikakis, M.; Iglesia, E. CO Activation Pathways and the Mechanism of Fischer-Tropsch Synthesis. J. Catal. 2010, 272, 287-297

(7) Mirwald, J.W.; Inderwildi, O. R. Unraveling the Fischer-Tropsch Mechanism: a Combined DFT and Microkinetic Investigation of C-C Bond Formation on Ru. Phys. Chem. Chem. Phys. 2012, 14 7028-7031

(8) Loveless, B.T; Buda, C.; Neurock, M.; Iglesia, E. CO Chemisorption and Dissociation at High Coverages during CO Hydrogenation on Ru Catalysts J. Am. Chem. Soc., 2013, 135, 6107-6121

(9) Hibbitts, D.D.; Loveless, B.T.; Neurock, M.; Iglesia, E. Mechanistic Role of Water on the Rate and Selectivity of Fischer-Tropsch Synthesis on Ruthenium Catalyts Angewandte Chemie., 2013, (52) 12273-12278

(10) Hibbitts, D.D.; Dybeck, E.; Lawlor, T.; Neurock, M.; Iglesia, E. Preferential Activation of CO Near Hydrocarbon Chains during Fischer-Tropsch Synthesis on Ru J. Catal., 2016. 337, 91-101

(11) Iglesia, E.; Reyes, S.C.; Madon, R.J.; Soled, S.L. Selectivity Control and Catalyst Design in the Fischer-Tropsch Synthesis: Sites, Pellets, and Reactors. Adv. Catal. 1993, 39, 221-302

(12) Bell, A.T. Catalytic Synthesis of Hydrocarbons over Group VIII Metals. A Discussion of the Reaction Mechanism. Catal. Rev. 1981,23,203-32

(13) Iglesia, E.; Reyes, S.C.; Madon, R.J. Transport-enhanced α-olefin Readorption Pathways in Ru-Catalyzed Hydrocarbon Synthesis J. Catal., 1991, 129, 238-256

(14) Madon, R.J.; Iglesia, E. The importance of Olefin Readsorption and H_2/CO Reactant Ratio for Hydrocarbon Chain Growth on Ruthenium Catalysts J. Catal., 1993, 139, 576-590

(15) Komaya, T.; Bell, A.T; Estimates of Rate Coefficients for Elementary Processes Occurring during Fischer-Tropsch Synthesis over Ru/TiO_2 J .Catal., 1993, 146, 237-248

(16) Herrington, E.F.G., The Fischer-Tropsch Synthesis Considered as a Polymerization Reaction. Chem. Ind. 1946, 65,346

(17) Yates, I.C.; Satterfield, C.N. Intrinsic Kinetics of the Fischer-Tropsch Synthesis on a Cobalt Catalyst. Energy Fuels 1991, 5, 168-173

(18) Brady, R.C. III.; Petit, R. Mechanism of the Fischer-Tropsch Reaction. The Chain-Propagation Step J. Am. Chem. Soc. 1981, 103, 1287-1289

(19) Brady, R.C. III.; Petit, R. Reactions of Diazomethane on Transition-Metal Surfaces and their Relationship to the Mechanism of the Fischer-Tropsch Reaction J. Am. Chem. Soc. 1980, 102, 6181-6182
(20) Maitlis, P.M.; Zanotti, V. Organometallic Models for Metal Surface Reactions: Chain Growth Involving Electrophilic Methylidynes in the Fischer-Tropsch Reaction Catal. Lett., 2007, 122, 80-83
(21)Maitlis, P.M.; Long H.C.; Quyoum, R.; Turner, M.; Wang, Z.Q. Heterogeneous Catalysis of C-C Bond Formation: Black Art or Organometallic Science? Chem. Commun. 1996, 1-8
(22) Turner, M.L.; Marsih, B.E.; Mann, R.; Quyoum, H.C.; Long, H.C.; Maitlis, P.M. Investigations by ^{13}C NMR Spectroscopy of Ethene-Initiated Catalytic CO Hydrogenation J. Am. Chem. Soc. 2002, 124, 10456
(23) van Santen, R.A.; Neurock, M., Molecular Heterogeneous Catalysis; Wiley-VCH: New York 2006
(24) Shetty, S.; Jansen, A.P.J.; van Santen, R. A. Direct versus Hydrogen-Assisted CO Dissociation. J. Am. Chem. Soc. 2009, 131, 12874-12875
(25) Ge, Q.; Neurock, M.; Wright, H.A.; Srinivasan, N. A First Principles Study of Carbon-Carbon Coupling over the [0001] Surfaces of Co and Ru. J. Phys. Chem. B 2002, 106, 2826-2829
(26) Zhuo, M.; Tan, K. F.; Borgna, A.; Saeys, M. Density Functional Theory Study of the CO Insertion Mechanism for Fischer-Tropsch Synthesis over Co Catalysts. J. Phys. Chem. C 2009, 113, 8357-8365
(27) van Santen, R.A.; Ciobica, I.M.; van Steen, E.; Ghouri, M. M. Mechanistic Issues in Fischer-Tropsch Catalysis. Adv. Catal. 2011, 54, 127-187
(28) Mirwald, J.W.; Inderwildi, O. R. Unraveling the Fischer-Tropsch Mechanism: a Combined DFT and Microkinetic Investigation of C-C Bond Formation on Ru. Phys. Chem. Chem. Phys. 2012, 14 7028-7031
(29) Carballo, J.M.G.; Yang, J.; Holmen, A.; Garcia-Rodriguez, S.; Rojas, S.; Ojeda, M.; Fierro, J.L.G. Catalytic Effects of Ruthenium Particle Size on the Fischer-Tropsch Synthesis. J. Catal., 2011, 284, 102-108
(30) dan Breejan, J.P.; Radstake, P.B.; Bezemer, G.L.; Bitter, J.H.; Froseth, V.; Holmen, A.; de Jong, K.P. On the Origin of the Cobalt Particle Size Effects in Fischer-Tropsch Catalysis J. Am. Chem. Soc., 2009, 131, 7197-7203
(31) Kresse, G.; Hafner, J. Ab Initio Molecular Dynamics for Liquid Metals Phys. Rev. B 1993, 47, 558
(32) Kohn, W. Sham, L. Quantum Density Oscillations in an Inhomogeneous Electron Gas. Phys. Rev. 1965, 137, 1697
(33) Perdew, J.P.; Chevrey, J.A.; Vosko, S.H.; Jackson, K. A.; Pederson, M.R.; Singh, D.J.; Fiolhais, C. Atoms, Molecules, Solids, and Surfaces: Application of the Generalized Gradient Approximation for Exchange and Correlation. Phys. Rev. B. 1976, 13, 5188
(34)Vanderbilt, D. Optimally Smooth Norm-Conserving Pseudopotentials. Phys. Rev. B. 1985, 32, 8412
(35) Monkhorst, H. J.; Pack, J.D. On Special Points for Brillouin Zone Integrations. Phys. Rev. B. 1976, 13, 5188

(36) Henkelman, G.; Jonsson, H. A Dimer Method for Finding Saddle Points on High Dimensional Potential Surfaces Using only the First Derivatives. J. Chem. Phys. 1999, 111, 7010
(37) Heyden, A.; Bell, A.T.; Keil, F. J. Efficient Methods for Finding Transition States in Chemical Reactions. Comparisons of Improved Dimer Method and Partitioned Rational Function Optimization Method. J. Chem. Phys. 2005, 123, 224101
(38) Kastner, J.; Sherwood, P. Superlinearly Converging Dimer Method for Transition State Search J. Chem. Phys. 2008, 128, 014106
(39) Johnson, H.; Mills, G.; Jacobsen K.W. Nudged Elastic Band Method for Finding Energy Paths of Transitions. Classical and Quantum Dynamics in Condensed Phase Simulations. World Scientific. Singapore, 1998, 385
(40) Henkelman, G.; Jonsson, H. Improved Tangent Estimate in the Nuded Elastic Band Method for Finding Minimum Energy Paths and Saddle Points. J. Chem. Phys. 2000, 113, 9978
(41) Chase, M.W., Jr. NIST-JANAF Thermochemical Tables, Fourth Edition, J. Phys. Chem. Ref. Data, Monograph 9, 1998, 1-1951
(42) Mims, C.A.; McCandlish, L.E. Evidence for Rapid Chain Growth in the Fischer-Tropsch Synthesis over Iron and Cobalt Catalysts. J.Phys. Chem. 1987, 91, 929-937
(43) 2014 Energy Technology Perspective, International Energy Agency

Appendix

Reaction	Rate Constant or Equilibrium Constant
Adsorption	
$CO + * \rightarrow CO*$	$K_{CO} = \exp\left(\frac{-\Delta G_{ads}}{RT}\right) = \frac{[CO*]}{P_{co}[*]}$
$H_2 + 2* \rightarrow 2H*$	$K_{H_2} = \exp\left(\frac{-\Delta G_{ads}}{RT}\right) = \frac{[H*]^2}{P_{H_2}[*]^2}$
Chain Growth	
$H_{2n+1}C_n* + CO* \rightarrow H_{2n+1}C_{n+1}O* + *$	$K_{C-C} = \exp\left(\frac{-\Delta G_{rxn}}{RT}\right) = \frac{[H_{2n+1}C_{n+1}O*][*]}{[H_{2n+1}C_n*][CO*]}$
$H_{2n+1}C_{n+1}O* + H* \rightarrow H_{2n+1}C_{n+1}* + OH*$	$k_{act} = \left(\frac{k_B T}{h}\right)\left(\frac{q^{TS}}{q_{H_{2n+1}C_{n+1}O*} q_{H*}}\right)\exp\left(\frac{-E_{act}}{RT}\right)$
Termination	
$H_{2n+1}C_n* + H* \rightarrow C_nH_{2n+2(g)} + 2*$	$k_t = \left(\frac{k_B T}{h}\right)\left(\frac{q^{TS}}{q_{H_{2n+1}C_n*} q_{H*}}\right)\exp\left(\frac{-E_{act}}{RT}\right)$
$H_{2n+1}C_n* + * \rightarrow C_nH_{2n(g)} + H* + *$	$k_o = \left(\frac{k_B T}{h}\right)\left(\frac{q^{TS}}{q_{H_{2n+1}C_n*} q_{*}}\right)\exp\left(\frac{-E_{act}}{RT}\right)$

Site Balance (CO* = MASI):

$$[L] = [*] + [CO*] \Rightarrow \frac{[*]}{[L]} = \frac{1}{(1 + K_{CO} P_{CO})}$$

Where [L]=the total number of sites.

$$[CO^*] = \mathrm{K}_{CO}\, P_{CO}[^*] \qquad [\mathrm{H}^*] = \mathrm{K}_{H_2}^{1/2}\, P_{H_2}^{1/2}[^*]$$

Rate of Propagation (n to n+1):

$$r_{p,n} = k_{act} K_{C-C}[H_{2n+1}C_n^*][CO^*][H^*]$$

Rate of Termination (n to n+1):

$$r_{t,n} = k_t[H_{2n+1}C_n^*][H^*] + k_o[H_{2n+1}C_n^*][^*]$$

Chain Termination Parameter:

$$\beta_n = \frac{r_{t,n}}{r_{p,n}} = \frac{k_t[H_{2n+1}C_n^*][H^*] + k_o[H_{2n+1}C_n^*][^*]}{k_{act}K_{C-C}[H_{2n+1}C_n^*]([CO^*]/[^*])[H^*]} = \frac{k_t[H^*] + k_o[^*]}{k_{act}K_{C-C}([CO^*]/[^*])[H^*]}$$

$$= \frac{(k_t K_{H_2}^{1/2} P_{H_2}^{1/2} + k_o)}{k_{act}K_{C-C}\,\mathrm{K}_{CO}\,K_{H_2}^{1/2}\,\mathrm{P}_{CO}\,P_{H_2}^{1/2}}$$

Chain Growth Probability: (assuming chain growth occurs via H*- assisted activation of acyls)

$$\alpha_n = \frac{r_{p,n}}{r_{p,n} + r_{t,n}} = \frac{k_{act}K_{C-C}\,\mathrm{K}_{CO}\,K_{H_2}^{1/2}\,\mathrm{P}_{CO}\,P_{H_2}^{1/2}}{k_{act}K_{C-C}\,\mathrm{K}_{CO}\,K_{H_2}^{1/2}\,\mathrm{P}_{CO}\,P_{H_2}^{1/2} + (k_t K_{H_2}^{1/2} P_{H_2}^{1/2} + k_o)}$$